Modeling Stochastic Chemical Kinetics on Quantum Computers

Tilas Kabengele,[1,2] Yash M. Lokare,[3] J. B. Marston,[3,4] and Brenda M. Rubenstein[1,3,a]

[1)]*Department of Chemistry, Brown University, Providence, Rhode Island 02912, USA*

[2)]*School of Engineering, Brown University, Providence, Rhode Island 02912, USA*

[3)]*Department of Physics, Brown University, Providence, Rhode Island 02912, USA*

[4)]*Brown Theoretical Physics Center, Brown University, Providence, Rhode Island 02912, USA*

(Dated: April 16, 2024)

The Chemical Master Equation (CME) provides a highly accurate, yet extremely resource-intensive representation of a stochastic chemical reaction network and its kinetics due to the exponential scaling of its possible states with the number of reacting species. In this work, we demonstrate how quantum algorithms and hardware can be employed to model stochastic chemical kinetics as described by the CME using the Schlögl Model of a trimolecular reaction network as an illustrative example. To ground our study of the performance of our quantum algorithms, we first determine a range of suitable parameters for constructing the stochastic Schlögl operator in the mono- and bistable regimes of the model using a classical computer and then discuss the appropriateness of our parameter choices for modeling approximate kinetics on a quantum computer. We then apply the Variational Quantum Deflation (VQD) algorithm to evaluate the smallest-magnitude eigenvalues, λ_0 and λ_1, which describe the transition rates of both the mono- and bistable systems, and the Quantum Phase Estimation (QPE) algorithm combined with the Variational Quantum Singular Value Decomposition (VQSVD) algorithm to estimate the zeromode (ground state) of the bistable case. Our quantum computed results from both noisy and noiseless quantum simulations agree within a few percent with the classically computed eigenvalues and zeromode. Altogether, our work outlines a practical path toward the quantum solution of exponentially complex stochastic chemical kinetics problems and other related stochastic differential equations.

I. INTRODUCTION

One of the most relevant yet underexplored applications of quantum computing in chemistry lies in chemical kinetics, which seeks to determine the transition rates and non-equilibrium steady states of a system by solving its the underlying stochastic differential equations (SDEs).[1] Since analytical solutions are limited to only a few special cases, numerical methods are typically employed to solve SDEs classically. However, due to the rapid expansion of their state space as their number of dimensions and degrees of freedom increase, solving SDEs is extremely challenging. For more exact approaches for solving SDEs such as the Chemical Master Equation (CME), the space complexity scales exponentially with the number of reacting species in the system. Quantum algorithms that can potentially overcome this classical scaling would thus enable the study of the dynamics of the larger, more complex reaction networks often found in biology,[2,3] chemical biophysics,[4] and atmospheric science.[5]

Several quantum algorithms for solving Ordinary Differential Equations (ODEs) and Partial Differential Equations (PDEs) have been developed over the years, including the Quantum Phase Estimation (QPE)[6] and the Harrow-Hassidim-Lloyd (HHL) algorithms.[7] Additionally, numerous quantum-classical hybrid algorithms suitable for Noisy Intermediate-Scale Quantum (NISQ)[8-10] computers have emerged in recent years. These algorithms typically utilize shallow quantum circuits, which are less prone to noise, and allocate part of the computation to a classical computer. Examples of such algorithms are Variational Quantum

Eigensolvers (VQEs),[11-13] the Variational Quantum Deflation (VQD) algorithm,[14] and the Variational Quantum Singular Value Decomposition (VQSVD) algorithm.[15] All of these algorithms involve classical optimization of a set of free parameters that define the variational ansätz (or, in other words, that are used to construct the parameterized quantum circuits needed to represent the quantum state). These parameters are then iteratively fed back into the quantum circuit until convergence is achieved. Variational quantum algorithms have been utilized to estimate the ground and excited states of small molecules such as H_2,[16-18] LiH,[16-18] HF,[16] and BeH_2,[19] as well as quantum magnets.[16] Recently, VQE was employed as a density matrix embedding solver in an *ab initio* simulation of strongly correlated materials.[20]

Although such variational quantum algorithms have existed for over a decade, the majority of research efforts have been focused on solving the Schrödinger Equation (SE).[21-24] However, many types of non-Schrödinger differential equations are related and can be transformed into one another under different approximations, opening up the possibility of leveraging quantum computers to also accelerate the solution of these equations, as has been discussed in recent seminal works.[25-28] In the context of stochastic processes, nearly all other types of stochastic differential equations can be transformed into the form of a Fokker-Planck Equation (FPE),[29,30] a partial differential equation that describes the evolution of a system's state variables in the presence of stochastic fluctuations. This includes the Master Equation, the Chapman-Kolmogorov Equation, and both Stratonovich's and Itô's Stochastic Differential Equations.[30,31]

In theory, the Chemical Master Equation is the ideal choice for modeling continuous-time stochastic processes in chemistry. The CME describes the evolution of the probability distribution of a system with discrete states in continuous

[a)]Electronic mail: Author to whom correspondence should be addressed: Brenda Rubenstein, brenda_rubenstein@brown.edu

time. The eigenvalues of the CME matrix provide information about transition rates and state lifetimes, while the corresponding eigenfunctions provide information about the state of the system, e.g., the long-term behavior and stability of a system can be described by the eigenfunction corresponding to the lowest eigenvalue.[32,33] The CME's solutions are typically considered exact since it considers all possible states. The CME is therefore a very resource-intensive approach due to the exponential explosion of the size of its state space with respect to the number of reacting species: a chemical system with N molecules, R reactions, and S reacting species requires an $[R(N+1)]^S \times [R(N+1)]^S$ stochastic matrix to fully capture all possible states. The CME can be approximated by an FPE-type equation in the rapid reaction rate limit in which chemical reaction rates are much faster than diffusion rates.[34,35] However, solving the CME directly is computationally prohibitive for the vast majority of applications outside the small population limit, even when numerical approximations such as uniformization and the Krylov subspace methods are applied.[36,37] Finding more efficient ways of solving the CME is still an active area of research in mathematics and computational science.[38]

Surprisingly, the CME has garnered little to no attention from the quantum computing community despite its significance in chemistry, biology, physics, and engineering and the computational hardships associated with solving it classically.[39,40] The closest effort to address the CME and chemical stochastic differential equations in general using quantum computing is perhaps the work by Pravatto *et al.*, in which the authors estimate the lowest non-zero eigenvalue of a Fokker–Planck-Smoluchowski operator describing the isomerization process in a chain of molecular rotors using a VQE approach.[41] This work's results confirm an increase in errors in the presence of noise and for larger basis sets, as also observed in quantum chemistry simulations.[42,43] However, there are fewer mitigation strategies available for classical chemical systems, as most mitigation strategies are typically designed with quantum chemistry in mind. For instance, it is well known that the technique used to map and encode a molecular Hamiltonian into qubits can significantly affect the performance of a quantum algorithm, yet most of the developed encoding schemes, including the Jordan–Wigner Transformation[44–46], Bravyi–Kitaev Transformation,[47,48] and Trotterization,[49–52] are designed for encoding and simulating quantum mechanical systems.[53] Similarly, more advanced versions of VQE that involve the adaptive, gradual growth of an ansätz, e.g., ADAPT-VQE,[54] are tailored to molecular Hamiltonians starting from a Hartree-Fock approximation. This lack of capabilities can be partially attributed to a limited appreciation of the potential of quantum algorithms for solving problems in classical chemistry, further compounded by the absence of demonstrations in the literature.

Our work aims to address some of these shortcomings by extending the application of quantum computing to classical chemical kinetics and analyzing the benefits it may bring and challenges it may face. We present a detailed analysis of the classical and quantum solutions to the Schlögl model,[55] a paradigmatic chemistry model describing the dynamics of a trimolecular autocatalytic process. The Schlögl model describes an inherently stochastic chemical reaction network and is therefore most accurately described by a CME. Owing to device constraints such as limited gate fidelity, gate crosstalk, and the ability to support only a few physical qubits,[9] solutions to the Schlögl model are possible only for a limited set of system parameters on current-NISQ computers. We discuss the suitable range of parameters for simulating this model and the rationale behind our parameter choices. We then apply VQD to determine the first two eigenvalues of our system in order to estimate rates and waiting times, and use a combination of QPE and VQSVD to approximate its steady state solution. We run our numerical simulations in Qiskit using a local simulator, the QASM simulator backend and `ibm_brisbane` with and without noise, and show that, for the first eigenvalue, the basis employed can be halved without sacrificing accuracy. Our results for both the eigenvalues and the non-equilibrium steady-state are in good agreement with classical results: notably, we obtain exact quantum-computed eigenvalues for the 2- and 3-qubit operator of the Schlögl model and root mean-squared (RMS) deviation errors as low as 3% for the quantum-computed non-equilibrium steady-state. Our work showcases the potential for quantum computing to solve classical chemistry problems and highlights the need for more efficient mapping and transformation techniques that are tailored to classical operators. To our knowledge, this is the first work to demonstrate the quantum simulation of classical chemical kinetics on near-term quantum hardware.

The rest of the paper is organized as follows: In Sec. II, we provide relevant background regarding the Chemical Master Equation and Schlögl model before describing the techniques we used to solve them on both classical and quantum hardware in Secs. III and IV. In Sec. V, we benchmark our results on both the noiseless (Qiskit) statevector simulator and `ibm_brisbane` against classical results, highlighting what simplifications can accurately be made along the way. Lastly, we contextualize our numerical results in Sec. VI and conclude with a future outlook in Sec. VII.

II. STOCHASTIC CHEMICAL KINETICS

Deterministic chemical kinetics are typically described using rate equations that predict the changes in concentrations of reacting species with time. However, in the presence of noise, e.g., due to fluctuations in the counts of particles for systems involving small molecular populations such as biochemical processes like DNA transcription, regulation,[56–58] and apoptosis,[59] a stochastic description of the reaction kinetics is required. The CME provides the most accurate but also the most computationally demanding approach to solving stochastic dynamics. This is due to the CME's high-dimensional state space, i.e., each chemical species considered in simulations adds a dimension to the CME.[36,60] Approximations can be made using the Chemical Fokker-Planck (CFPE) and the Chemical Langevin Equations (CLE),[61] and stochastic numerical approaches have been developed such as Gillespie's stochastic simulation algorithm (SSA).[62] How-
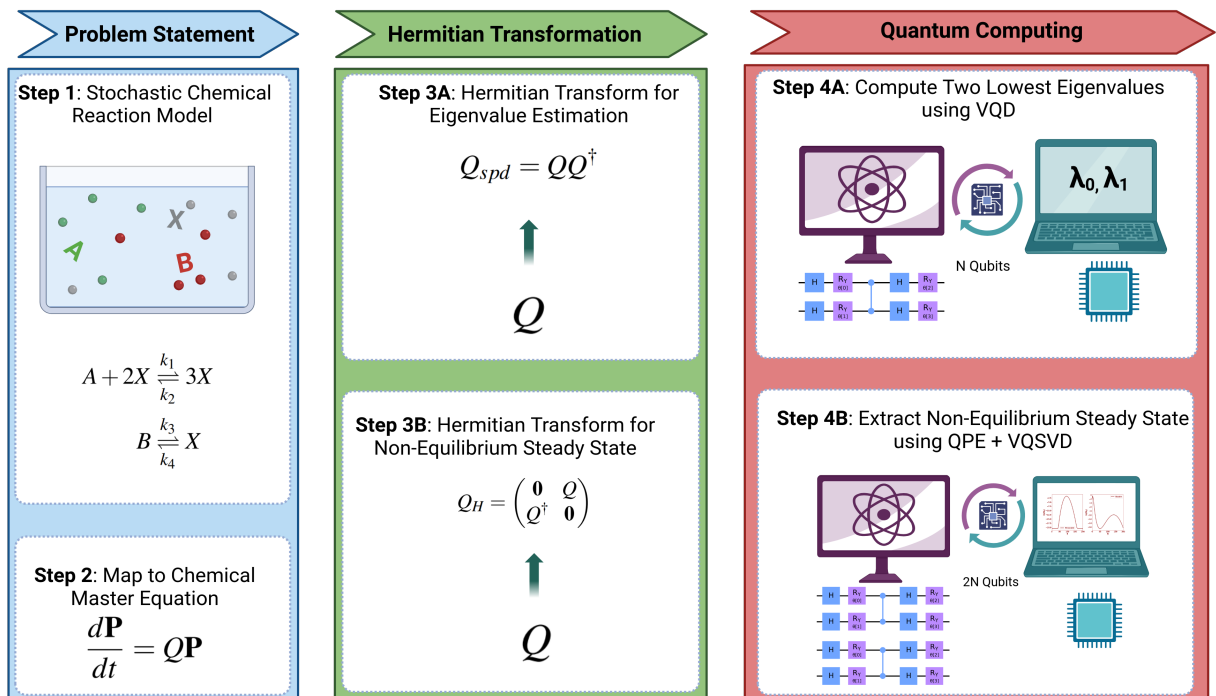
Figure 1: Overview of the workflow presented in this manuscript. In **Step 1**, a stochastic chemical reaction network is given as the problem statement. The reaction network is then mapped to a Chemical Master Equation with stochastic matrix Q in **Step 2**. In **Step 3**, the stochastic matrix is converted to Hermitian form. Finally, in **Step 4**, the two lowest eigenvalues and the non-equilibrium steady state are computed using variational quantum algorithms.

ever, like any Monte Carlo-based simulation method, the sampling error in SSA can be very challenging to estimate and its convergence may be very slow for large systems or rate constants.[33] Meanwhile, the CFPE and CLE can yield inaccurate results outside of the thermodynamic limit and for systems with small volumes, e.g., biochemical reactions inside a cell.[35,63–65] Our work presents a proof-of-concept alternative to solving the CME on near-term quantum hardware.

A. Chemical Master Equation

The CME is an ODE describing the evolution of a continuous time, discrete space Markov process. In the context of biochemical reactions, it describes a system of N spatially homogeneous molecular species $\{S_1, S_2, ..., S_N\}$ interacting through M chemical reaction channels $\{R_1, R_2, ..., R_M\}$ at a constant volume and in thermal equilibrium. If we denote the number of S_i molecules in the system at time t by $X_i(t)$, where $i = (1, 2, ..., N)$, the molecular population vector is given by $\mathbf{X}(t) \equiv (X_1(t), X_2(t), ..., X_N(t))$, where $\mathbf{X}(t)$ changes stochastically due to the presence of noise in the system. Rigorous derivations of the CME[35,61,66] show that, if the reacting species are confined to a specific volume, kept well-stirred, and held at a constant equilibrium temperature, the probability for one reaction R_j to occur in the system in the next infinitesimal time interval $[t, t + dt)$ is given by

$$P(\mathbf{x}, t | \mathbf{x}_0, t_0) = a_j(\mathbf{x}) dt, \tag{1}$$

where a_j is the propensity function, $j = (1, 2, ..., M)$, and $\mathbf{X}(t) = \mathbf{x}$ is an N-dimensional *Markov jump process*, i.e., $\mathbf{X}(t)$ executes a *random walk* in the N-dimensional state space. Thus, for each j, a state-change vector

$$\mathbf{v}_j \equiv (v_{j1}, v_{j2}, ..., v_{jN}) \tag{2}$$

is defined using the change in the number of S_i molecules as a result of one reaction R_j. Given an initial probability $P(\mathbf{X}_0, t_0)$ and that $t \geq t_0$, the time evolution of the probability function satisfies Equations 1 and 2 and is given by the CME[35]

$$\frac{d}{dt}P(\mathbf{x}, t | \mathbf{x}_0, t_0) = \sum_{j=1}^{M} [a_j(\mathbf{x} - \mathbf{v}_j)P(\mathbf{x} - \mathbf{v}_j, t | \mathbf{x}_0, t_0) \\ - a_j(\mathbf{x})P(\mathbf{x}, t | \mathbf{x}_0, t_0)]. \tag{3}$$

The CME has been rigorously shown to be an exact description of the microscopic physics of a system as it considers every possible state by taking into account all the possible reactions. For sufficiently large molecular populations, the CME can be approximated by a CLE, CFPE, or a reaction rate equation (RRE), which all assume a continuous Markov process. For a detailed discussion of the relationship between the CLE, CFPE, and RRE to the CME, we direct the reader to Refs. 35,61,66.

B. The Schlögl Model

The Schlögl model,[55] named after its author, F. Schlögl, is a chemical reaction network that, in its stochastic form, exhibits bistability. The model was first developed to understand non-equilibrium phase transitions in well-stirred chemical reactions by analyzing the steady and unstable states of a system with respect to the concentrations of the reacting species.

Due to the inherent randomness of the collisions of the molecules in a stirred mixture, the kinetics of a well-stirred chemical composition can be modeled using stochastic differential equations. If the system comprises a considerable number of particles, or in statistical mechanics terminology, approaches the thermodynamic limit of infinite molecular populations, the Langevin and Fokker-Planck stochastic differential equations can be used. However, the CME is more suitable if the system is characterized by small molecular populations, as is the case in cellular biological systems and biochemical processes.[61,67] In the Schlögl model, the concentrations of some of the species are kept constant while the concentrations of other species are allowed to change. The species with variable concentrations are referred to as dynamic species. The Schlögl model can be deterministic or stochastic depending on whether the concentration of the dynamic species is allowed to fluctuate randomly or according to a predictable pattern. If we let A and B signify the constant species and X the dynamic species, a simple Schlögl model will be given by the reaction network[32,55]

$$A + 2X \underset{k_2}{\overset{k_1}{\rightleftharpoons}} 3X \tag{4a}$$

$$B \underset{k_4}{\overset{k_3}{\rightleftharpoons}} X \tag{4b}$$

where k_1, k_2, k_3, and k_4 are rate constants. The deterministic Schlögl model can be obtained using the law of mass action,[68] which posits a direct relationship between the rates of a chemical reaction and the concentrations of its reacting species. Let a and b be the concentrations of the static species and x be the concentration of the dynamic species. The deterministic Schlögl model for the reactions above can be written in the form of an ordinary differential equation[32]

$$\frac{dx}{dt} = k_1 a x^2 - k_2 x^3 - k_4 x + k_3 b. \tag{5}$$

The stochastic Schlögl model is described by a CME with infinitely-coupled ODEs truncated at some finite number N for numerical purposes. It can be derived by first defining the number of molecules of A, B, and X in a fixed volume V. Let n_A and n_B be the number of A and B molecules, and $n_X(t)$ be the number of X molecules at time t. From here, one can define a probability distribution function $P_n(t)$ that gives the probability of finding n number of X molecules at time t. The stochastic Schlögl model will then be governed by a

birth-death Markov process with the following CMEs:

$$\frac{dP_0(t)}{dt} = \mu_1 P_1 - \kappa_0 P_0, \tag{6a}$$

$$\frac{dP_n(t)}{dt} = \kappa_{n-1} + \mu_{n+1} P_{n+1} - (\kappa_n + \mu_n) P_n, \tag{6b}$$

where $n = [1, \infty)$, i.e., the stochastic model constitutes an infinite system of coupled ordinary differential equations. Here, κ_n and μ_n are known as the birth and death rates of the Markov process, respectively. They are the recurrence relations used to construct the stochastic matrix and may be written in terms of the deterministic rate constants k_1, k_2, k_3, and k_4, and the volume V of the system:[32]

$$\kappa_n = \frac{a k_1 n(n-1)}{V} + b k_3 V, \tag{7a}$$

$$\mu_n = n k_4 + \frac{k_2 n(n-1)(n-2)}{V^2}. \tag{7b}$$

C. Discretization Procedure

Discretizing the Schlögl model is relatively straightforward since the CME is a discrete differential equation. All we need to do is cast Equation 6 into a matrix by taking into account the recurrence relations given by Equation 7. The goal is to obtain the stochastic matrix, Q, that describes the Schlögl model through the following stochastic differential equation:

$$\frac{d\mathbf{P}}{dt} = Q\mathbf{P} \tag{8}$$

where each component of the vector $\mathbf{P}$ represents the probability for each state. The solution $\mathbf{P}(t)$ can then be given in terms of the eigenvectors and eigenvalues of Q as follows:

$$\mathbf{P}(t) = c_0 \mathbf{v}_0 e^{\lambda_0 t} + c_1 e^{\lambda_1 t} \mathbf{v}_1 + ..., \tag{9}$$

where $(\lambda_0, \lambda_1, ...)$ are the eigenvalues and $(\mathbf{v}_0, \mathbf{v}_1, ...)$ are the *right* eigenvectors of Q. The vector $\mathbf{v}_0$ corresponds to the lowest eigenvalue and represents the steady state solution (i.e., $\frac{d\mathbf{P}}{dt} = 0$) of the system. The stochastic matrix Q has an infinite form[32]

$$Q = \begin{pmatrix} -\kappa_0 & \mu_1 & 0 & \cdots \\ \kappa_0 & -\kappa_1 - \mu_1 & \mu_2 & \cdots \\ 0 & \kappa_1 & -\kappa_2 - \mu_2 & \cdots \\ \vdots & \vdots & \vdots & \cdots \end{pmatrix}, \tag{10}$$

but, in practice, must be truncated at a finite number, N, such that $\kappa_N = 0$ and $\mu_{N+1} = 0$. Q has real and negative eigenvalues starting from $\lambda_0 = 0$. Since $\mathbf{v}_0$ corresponds to the zero eigenvalue, it is also known as the zeromode. Figure 2 shows the zeromode of the Schlögl model for various sets of parameters. These steady states give the long-term behavior of the system. The stochastic nature of the Schlögl model can be seen through the existence of a bistable regime when the equilibrium condition given by Equation 20 is not satisfied (see Figure 2(b)). This non-equilibrium steady state is characterized

by two peaks separated by a trough (an unstable steady state) corresponding to two different states in which the system is likely to be, e.g., the two states in which a cell performs its functions.[32] As shown in Figure 2(b), one of the peaks will be more dominant than the other, i.e., will have a higher probability. However, since the trough corresponds to a non-zero value on the y-axis, there is a non-zero probability of transitioning to the other steady state, i.e., the non-dominant peak. Given that these *functional* states have unequal probabilities, the bistable Schlögl model predicts that the system will spend more time in one state than the other. An important quantity one can extract from the stochastic matrix Q is its smallest non-zero eigenvalue denoted by λ_1, which is directly proportional to the transition rate but inversely related to the waiting time (i.e., time spent in a functional state). Let r^+ and r^- represent the transition rates from the dominant peak to the non-dominant peak and vice versa, respectively. If we denote the waiting times in the dominant and non-dominant states by T^+ and T^-, respectively, λ_1 is defined as[69]

$$\lambda_1 = r^+ + r^- = -\frac{1}{2T^+} - \frac{1}{2T^-}. \tag{11}$$

In the bistable case, the magnitude of λ_1 decays exponentially as V increases, which means that for larger volumes, distinguishing between λ_0 and λ_1 is more challenging. From Figure 2(b), it can also be seen that the bistability of the system becomes more apparent as the volume increases. As illustrated in Figure 2, a larger basis is required to represent steady states with larger volumes. From Figure 2(b), it can be seen that the bistability becomes more pronounced for larger volumes. The eigenvalues follow a similar trend: as V increases, λ_1 approaches λ_0 such that the states become indistinguishable. This results in a steady steady with two peaks.

D. Computational Complexity of Solving the Chemical Master Equation

The greatest challenge to numerically solving the CME is the rapid expansion of its state space with the number of reacting species S, number of reaction channels R, and the maximum count of molecules per species N. In terms of the above, the total number of possible states in the system is given by

$$\mathcal{N} = [R(N+1)^S], \tag{12}$$

which includes the zero state in which a particular molecule is absent or completely used up. The stochastic matrix representing such a system will therefore have dimensions

$$\mathcal{M} = [R(N+1)^S] \times [R(N+1)^S], \tag{13}$$

i.e., its dimensionality grows exponentially with the number of reacting species, S. Exact diagonalization typically scales as $\mathcal{O}(\mathcal{N}^3)$, where $\mathcal{N}$ denotes the dimension of the matrix in question. Therefore, solving a CME by exact diagonalization may carry a space complexity of $\mathcal{O}((N+1)^{3S})$, which is intractable for most systems encountered in chemistry. The vast majority of numerical approaches for solving the CME therefore strive to alleviate this *curse of dimensionality*[70] by using state space reduction methods such as the Krylov subspace and uniformization methods.[36,57] Krylov subspace methods involve iteratively growing the state space by finding *subspaces* that represent the original system while uniformization approaches attempt to solve a transformed CME with uniform transition rates. Obtaining exact solutions to chemical dynamics problems like the ones highlighted in this work is thus exponentially costly on classical computers, making these systems potential targets of opportunity for quantum algorithms; the techniques described below attempt to take a step in this direction.

III. METHODS

A. Hermitian Transformations

To solve this problem using variational quantum eigensolvers fit for near-term quantum architectures,[9] the matrix 10 must be transformed into Hermitian form so that the first and second eigenstates can be distinguished by virtue of them being orthogonal to each other. The Hermitian form of Equation 10 can be obtained through the transformation

$$Q_H = \begin{pmatrix} \mathbf{0} & Q \\ Q^\dagger & \mathbf{0} \end{pmatrix}, \tag{14}$$

where $\mathbf{0}$ denotes the zero matrix and $Q^\dagger$ is the conjugate transpose of Q. The matrices 10 and 14 are connected by a singular value decomposition such that the eigenvalues of Equation 14 are the singular values of Equation 10. The singular values are not generally similar to the eigenvalues; however, for matrices that are nearly Hermitian, the singular values will be proportional to the eigenvalues. Equation 14 can thus be considered a Hermitian approximation to the non-Hermitian stochastic problem 8. Figure 4 shows the classically computed eigenvalue of the Schlögl model for different values of V. We show that the non-Hermitian eigenvalues of the bistable system are a good approximation to the eigenvalues of the original operator. For volumes between 0.1 and 20.1 in steps of 1.0, we obtained a root mean squared error (similar to Equation 21) of 0.15 for λ_1 between the Hermitian and non-Hermitian operators. In the same volume range, we obtained a coefficient of determination, R^2, of 0.95. R^2 was computed using

$$R^2 = 1 - \frac{\sum_i \left(y_i^{\text{classical}} - y_i^{\text{quantum}}\right)^2}{\sum_i \left(y_i^{\text{classical}} - y_{\text{mean}}^{\text{classical}}\right)^2}, \tag{15}$$

where $y_i^{\text{classical}}$, y_i^{quantum}, and $y_{\text{mean}}^{\text{classical}}$ denote the eigenvalues obtained classically, via quantum algorithms (VQD), and the mean of the classically obtained eigenvalues, respectively. In our quantum simulations, we therefore focus on the eigenvalues of the bistable system and obtain the zeromode (non-equilibrium steady-state) in this regime of the Schlögl model.
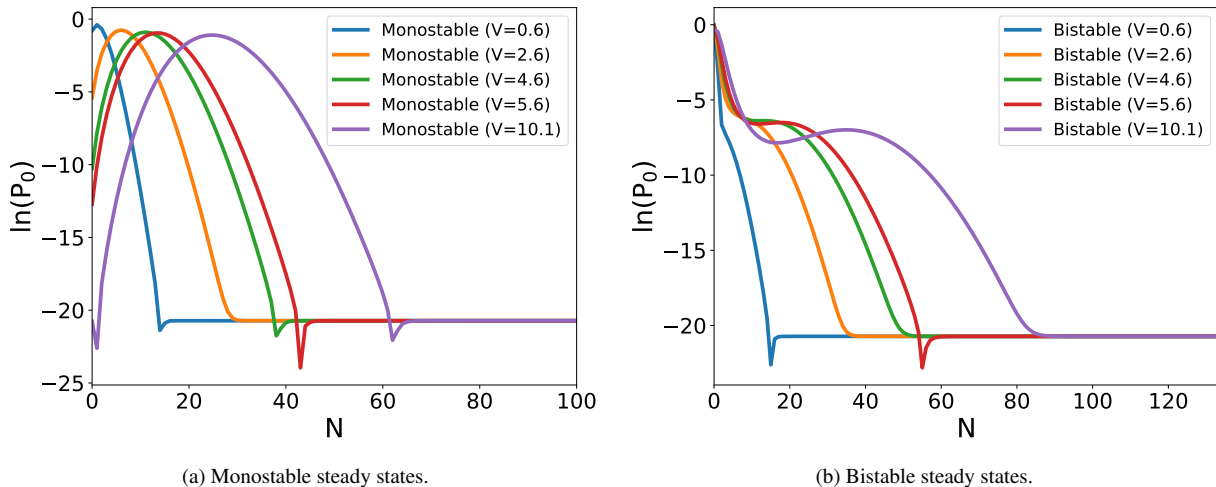
6

(a) Monostable steady states.

(b) Bistable steady states.

Figure 2: Monostable and bistable steady states of the Schlögl model as a function of the basis size, N, for different volumes, V. The monostable steady state is characterized by a Poisson distribution with a single peak while the bistable case is characterized by a deformed Poisson-like distribution with two peaks separated by a trough. All plots are given on a log scale.

Note that Equation 14 requires a basis size twice as large as the original operator. Although the eigenvectors of the original operator are essentially conserved in this transformation, the first (left) half of the components in the computed eigenvectors must be discarded as shown in Figure 3. The first half of the zeromode (steady state) of the Hermitian operator is an artifact of the **0** matrices used in the transformation—only the latter (right) half of the eigenvector components carry information about the steady state. In our quantum simulations, we used this transformation to recover the zeromode of the Schlögl operator using QPE and VQSVD. For the eigenvalue simulations with VQD, we use the Cholesky decomposition

$$Q_{spd} = QQ^{\dagger}, \qquad (16)$$

which ensures that the Schlögl operator is semi-positive definite. The eigenvalues of Q_{spd} are the squares of the singular values of Q without the negative sign, since Q_{spd} has only non-negative eigenvalues. Provided the initial matrix is not too far from Hermitian, one can therefore still approximate the eigenvalues of Q using Equation 16. Note that Equation 16 does not conserve the eigenvectors like Equation 14. However, its smaller basis size makes it more ideal for eigenvalue simulations using VQD. Since the eigenvalues using VQD are computed one after the other starting from the smallest to the largest, the operator Q_H has twice as many eigenvalues. Therefore, it would take twice as many iterations to get to a desired eigenvalue compared to using Q_{spd}. Perhaps most importantly for this work, we numerically identify a relationship between the zeromodes of Q_{spd} and Q. Specifically, the zeromode of Q_{spd} is exactly equal to the *left* eigenvector of Q corresponding to λ_0. This allows us to implement a modified version of the VQD algorithm, VQD-`exact0`, which skips the first state and directly computes λ_1. Using an exact initial state for the VQD algorithm also allows us to retrieve an exact first

excited state of Q_{spd} corresponding to the eigenvalue λ_1. The exact initial vector of Q_{spd} used in our simulations is the constant state given by

$$\mathbf{w}_0 = \underbrace{\left[\frac{1}{2^N}, \frac{1}{2^N}, \frac{1}{2^N}, \cdots \frac{1}{2^N}\right]^T}_{\text{Length}=2^N}, \qquad (17)$$

where N is the number of qubits needed to encode Q_{spd}. Since $\mathbf{w}_0$ has a length of 2^N, it is normalized to unity by dividing by this length.

B. VQD

VQD is a variational quantum algorithm that estimates the excited state energies of a particular Hamiltonian.[14] In our numerical simulations, we use VQD to compute the lowest and second lowest eigenvalues of the stochastic Schlögl matrix.

Given a Hermitian operator (or Hamiltonian), $\hat{H}$, VQD takes in as input a specified number k of the eigenvalues of $\hat{H}$. The objective of VQD is to first find a parameter λ_0 such that the cost function

$$E(\lambda_0) = \langle \psi(\lambda_0)|\hat{H}|\psi(\lambda_0)\rangle, \qquad (18)$$

is minimized. Once we determine λ_0 using the variational quantum eigensolver algorithm,[11,71] we adopt an iterative procedure to find parameters λ_1 through λ_k such that the cost function,

$$F(\lambda_x) = E(\lambda_x) + \sum_{i=0}^{x-1} \beta_i |\langle \psi(\lambda_x)|\psi(\lambda_i)\rangle|^2, \qquad (19)$$

is minimized $\forall\, x \in [1,k]$ (here, $\beta_i \in \mathbb{R}$). We decompose the Hamiltonian $\hat{H}$ into a linear combination of Pauli strings, i.e.,

(a) Hermitian Schlögl matrix at $V = 33$.
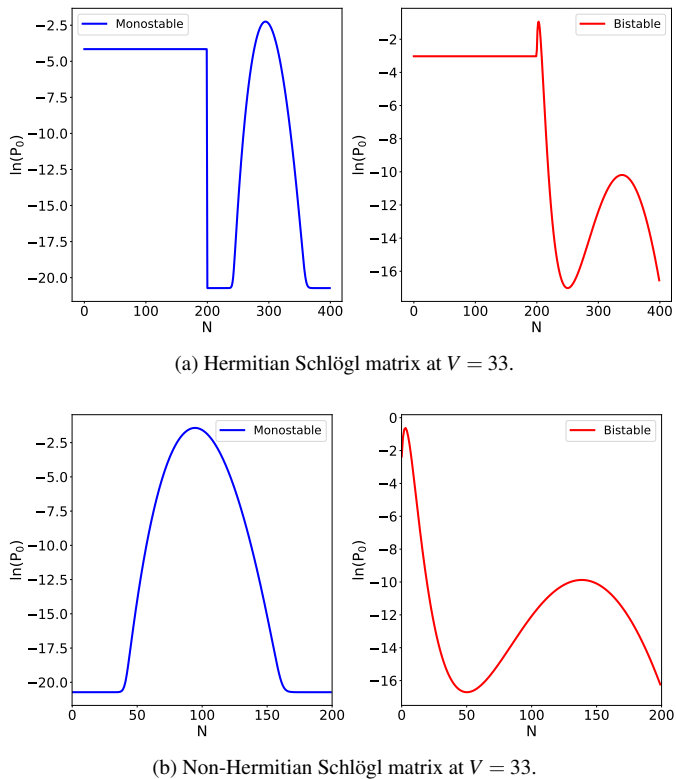

(b) Non-Hermitian Schlögl matrix at $V = 33$.

Figure 3: (a) Monostability (left) and bistability (right) of the Schlögl model at $V = 33$. The rate constants for both the monostable and bistable systems are as follow: $k_1 = 3$; $k_2 = 0.6$; $k_3 = 0.25$; and $k_4 = 2.95$. The pump parameters for the monostable state are $a = 0.5$ and $b = 29.5$. For the bistable state, $a = b = 1$.[32] (b) Same as (a), but for a non-Hermitian Schlögl operator.

$\hat{H} = \sum_j c_j \hat{P}_j$, to facilitate the implementation of VQD on near-term quantum hardware.

C. QPE

QPE is a quantum algorithm that estimates the eigenvalues of an unitary matrix.[72] Here, we use QPE as a consistency check, i.e., to verify if the stationary state of the stochastic Schlögl model can be recovered by a quantum algorithm. Furthermore, we use QPE to estimate the minimum eigenvalue (denoted as $\lambda_{\min}$ for the purpose of discussion) of the unitary representation of the stochastic Schlögl matrix. We use $\lambda_{\min}$ in conjunction with VQSVD to obtain an estimate for the non-equilibrium steady-state of the Schlögl model (see Sec. III D for more details).

D. Non-Equilibrium Steady State from VQSVD

We use VQSVD to obtain an estimate for the non-equilibrium steady-state (or zeromode) of the stochastic (bistable) Schlögl matrix. One amongst the several goals of singular value decomposition (SVD) is to examine the null space of any given matrix. SVD seeks to find a decomposition of the form $UDV^{\dagger}$ for some arbitrary matrix T, where U and V contain the left and right singular eigenvectors of T, respectively, and D is a diagonal matrix that encodes information about the singular values of T.

Current-NISQ devices are capable of supporting only a limited number of physical qubits. One designs variational quantum algorithms by keeping such constraints in mind, i.e., a limited gate fidelity and the ability to support only a few physical qubits on NISQ hardware.[15] To this end, we employ VQSVD,[15] a variational quantum algorithm that seeks to implement SVD via an optimization procedure. A detailed discussion of the implementation of VQSVD is beyond the scope of this work (we direct the reader to Ref. 15 for more details).

Finding the non-equilibrium steady-state—We compute the non-equilibrium steady-state of the stochastic Schlögl model following an eigenvalue equation treatment of the zeromode. We briefly outline the steps involved in obtaining an estimate for the non-equilibrium steady-state, as also illustrated in Fig. 1, below:

- Construct a finite volume discretization (i.e., a matrix representation) for the Schlögl operator using the procedure outlined in Sec. II C. Thereafter, apply a block-diagonal transformation to this matrix (we denote this as Q_H for the purpose of discussion; also see Sec. II C).

- Construct the unitary representation of the Hermitian matrix Q_H (i.e., $U = e^{-iQ_H}$). As discussed in Sec. III A, this transformation preserves the eigenvector spectrum of the Schlögl operator.

- Search the null space of the matrix $U - \lambda_{\min} I_{d \times d}$ using VQSVD to obtain an estimate for the non-equilibrium steady-state. As mentioned earlier, this realization follows from the fact that U and Q_H share the same eigenvector spectrum as they are connected via a unitary transformation. We use QPE to estimate $\lambda_{\min}$.

IV. IMPLEMENTATION

We implement VQD, QPE, and VQSVD using the Qiskit platform.[73] The `TwoLocal` ansätz was used in all of our VQD simulations. For the 2- and 3-qubit operators, we used the 1- and 2- circuit repetitions of R_Y gates with linear CNOT entanglements, respectively. For the 4-qubit operator, similar ansätzë labeled as A and B, were used with 4- and 5- circuit repetitions. The number of circuit parameters ranged from 4 (for the 2-qubit operator) to 24 (for ansätz B). The classical optimization of the parameters was performed using the Limited-Memory Broyden-Fletcher-Goldfarb-Shanno Bound (L-BFGS-B)[74] algorithm available in the Qiskit package. All VQD implementations were noiseless using local simulators of Qiskit's `Estimator`, `Sampler`, and `StateVector` classes. For QPE, we ran numerical experiments on `ibm_brisbane`, a publicly-available 127-qubit quantum processing unit (QPU). We determined the number of qubits used to construct the

query qubit register by $n = \log_2(d)$, where d denotes the dimension of $\hat{U}$, the unitary representation of the block diagonal form of the stochastic Schlögl matrix (we denote this as Q_H in the preceding sections). To construct $\hat{U}$, we performed the unitary transformation $\hat{U} = e^{-iQ_H}$ (the eigenvector spectrum of Q_H is preserved under this unitary transformation). We used QPE to estimate the minimum eigenvalue of $\hat{U}$.

We set the number of precision qubits used to construct the precision qubit register equal to seven across all experimental runs. We set the optimization level of the QPE circuit equal to 1 throughout to allow for minimal optimization of the QPE circuit.

Next, we employ VQSVD[75] (implemented on the PaddlePaddle Deep Learning platform[76,77]) to obtain an estimate for the zeromode of the stochastic Schlögl matrix. We use the hardware-efficient $R_Y - R_Z$ ansätz, which consists of single-qubit rotation gates and two-qubit entangling CNOT gates (we direct the reader to Ref. 15 for more details regarding the ansätz architecture). We use the Adam optimizer to perform a classical optimization of the variational parameters. We choose the weights to run VQSVD per the procedure outlined in Ref. 15. Further details pertaining to the setup and implementation of VQSVD may be found in the Supplementary Materials.

V. NUMERICAL RESULTS

A. Parameter Selection

a. Rate Constants The Schlögl model can exhibit monostability or bistability depending on the number of species and parameters chosen. Information about the stability of the system can be directly obtained from the steady state solution or the zeromode, i.e., the eigenvector corresponding to the zero eigenvalue (see Figure 2). The monostable Schlögl model is characterized by a Poisson distribution with a single peak corresponding to the concentration of the dynamical species x required to achieve chemical equilibrium.[30,78] To achieve chemical equilibrium, *chemical detailed balance* must be satisfied, i.e., the forward fluxes J_i^+ must equal the backward fluxes J_i^- across the entire reaction network ($J_i^+ = J_i^-$). The equilibrium condition for the Schlögl model will then be given by

$$\frac{R_\rightarrow}{R_\leftarrow} = \frac{k_1 k_4 a}{k_2 k_3 b} = 1, \tag{20}$$

where $R_\rightarrow$ and $R_\leftarrow$ denote the forward and backward reaction rates in the system, respectively.

On the other hand, the bistable Schlögl model signifies a departure from equilibrium and is characterized by a deformed Poisson-like distribution with two peaks. Each peak corresponds to a stable steady state, with an unstable steady state (the trough) between them. Since the bistable system is only achieved when the equilibrium condition given by Equation 20 is not satisfied, each steady state (peak) is actually a non-equilibrium steady state (NESS). Consequently, the bistable system can oscillate and evolve between two NESSs

since there is a non-zero probability of moving from one stable state to the other. In principle, any set of parameters that satisfy (violate) Equation 20 will result in a monostable (bistable) solution. In this work, we chose a set of parameters that illustrated a clear distinction between the monostable and bistable regimes and that had been previously studied analytically. Following Ref. 32, the rate constants used throughout this work are as follows: $k_1 = 3$; $k_2 = 0.6$; $k_3 = 0.25$; and $k_4 = 2.95$. To satisfy Equation 20 and achieve monostability, we set $a = 0.5$ and $b = 29.5$. The bistable case was realized using $a = b = 1$. Note that varying a and b while keeping other parameters constant would shift the relative heights of the NESS in Figure 2(b). Since the birth and death rates given by Equation 7 are scaled by V, the system volume is also critical in describing bistability.

b. System Volume Figure 4 shows the effects of changing the volume on the eigenvalues of the monostable and bistable Hermitian and non-Hermitian Schlögl models. For the bistable system, the Hermitian and non-Hermitian results for λ_1 vary only slightly compared to the monostable case. For larger volumes, the bistable eigenvalues are almost indistinguishable due to the exponential decay of λ_1—both the Hermitian and non-Hermitian λ_1 values approach zero when V is very large. For example, setting $V = 100$ gives $\lambda_1 \approx 10^{-10}$, while setting $V = 1$ yields $\lambda_1 \approx 1.5$. In order to get a first excited state, i.e., λ_1, that is sufficiently distinguishable from the ground state, λ_0, the volume must satisfy: $V \rightarrow 0$ (see Figures 4a and 4b). Nevertheless, the Hermitian approximations discussed in Section III A can provide a reasonable estimate of the Schlögl eigenvalues for the bistable system, particularly for moderate volumes, e.g., V in the range $0.5 - 30$. We note that simulating systems with very large or very small volumes is still a challenging task for variational quantum algorithms due to the limited precision available on current NISQ hardware—variational quantum algorithms must be able to distinguish between the eigenvalues of orthogonal states to reliably compute the desired eigenvalues and eigenvectors of the system.

B. Eigenvalues

a. Classical Eigenvalues Figure 4 shows the eigenvalues computed using exact diagonalization of the Hermitian and non-Hermitian Schlögl operators. In the bistable case, λ_0 and λ_1 become indistinguishable for very small or very large volumes.

b. Quantum Eigenvalues The first two lowest eigenvalues for the Hermitian bistable Schlögl model were computed using VQD. The 2-, 3-, and 4-qubit operators were used to approximate the Schlögl operator as shown in Figure 5. These operators were first converted to Hermitian form using Equation 16 and then decomposed into Pauli strings. The quantum computed eigenvalues are in excellent agreement with the classical (Hermitian) eigenvalues for the 2- and 3-qubit operators. The errors observed in the 4-qubit operator case can be attributed to a combination of a poor ansätz and the computational difficulty of optimizing variational parameters for a
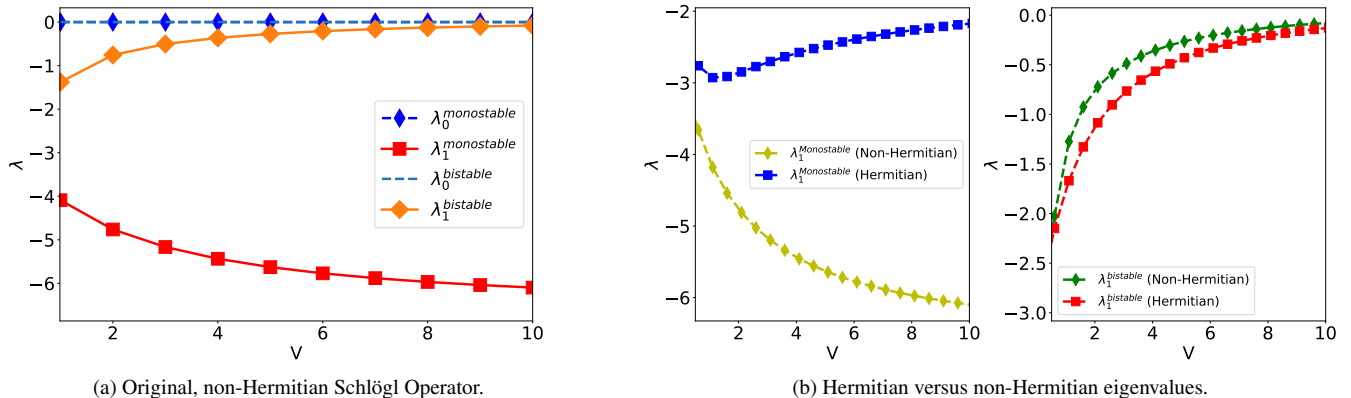
(a) Original, non-Hermitian Schlögl Operator.

(b) Hermitian versus non-Hermitian eigenvalues.

Figure 4: Classically-computed eigenvalues of the Schlögl operator for different volumes. (a) λ_0 and λ_1 from the original, non-Hermitian Schlögl operator. (b) A comparison of the Hermitian and non-Hermitian values of λ_1. The gap between the monostable solutions is relatively small when V is tiny, but continues to grow steadily as V increases. In the bistable case, the Hermitian solution approaches the solution to the original non-Hermitian Schlögl problem in the very large or very small volume limits. However, for large volumes, e.g., $V \gg 10$, numerical instabilities arise and quickly make the problem intractable. Similarly, setting $V = 0$ is not only numerically impractical but also devoid of any physical meaning.

large circuit – both well-known issues in the literature.[8,10,79] For context, the 2-qubit ansätz had only 4 variational parameter to optimize, while the 4-qubit ansätz had up to 24 parameters.

For the 2- and 3-qubit operators, various sorting techniques were adopted to analyze which terms can be omitted from the operator in order to boost our computational efficiency without significantly sacrificing accuracy. In the positive-first sort, terms were arranged from largest to smallest, starting with positive values. In the default sort, no modifications were made to the order of the terms after applying the Pauli decomposition algorithm in Qiskit. In the magnitude sort, the Pauli terms were arranged in order of the magnitudes of the coefficients of the Pauli terms. In the optimized sort, only terms that give non-zero expectation values with respect to the known initial state given in Equation 17 were used. Since optimized sort requires classically computing the expectation values of each Pauli term, it was only used as an additional check to understand what the most important terms were for an exact evaluation of λ_0. Figure 6 shows the errors on the associated quantum computed eigenvalues. Table S4 in the Supplementary Materials shows the lowest percent errors obtained for each sorting technique. For λ_0, default sorting the Pauli terms and using only $\sim 50\%$ of them was sufficient to obtain an exact solution. We empirically found that the expectation values of at least the latter half of any operator were zero and, thus, did not contribute to λ_0. This was not the case for λ_1 since all the expectation values were non-zero. Nonetheless, we found that for λ_1, sorting the operators by the magnitude of their coefficients gave the most favorable trade-off between accuracy and the number of terms truncated from the original operator. As shown in Table S4 in the Supplementary Materials, using 24/28 terms resulted in an error of 1.29% for the 3-qubit operator and using 7/10 terms resulted in a 0% error in λ_1 for the 2-qubit operator.

c. VQD-exact0 Finally, we computed the eigenvalues for all three operators using VQD with an exact initial state (we label this implementation as VQD-exact0). We utilized our knowledge of the zeromode of the Hermitian operator given by Equation 16 to accelerate the convergence of VQD. Specifically, we used Equation 17 as the VQD initial "guess" and observed a significant reduction in the number of VQD iterations. Figure 7 shows the convergence of λ_0 and λ_1 for 2-, 3-, and 4-qubit operators from our noiseless simulations. Exact values for λ_0 and λ_1 were obtained with VQD-exact0 in less than half the number of iterations needed by standard VQD. Additionally, highly accurate representations of the eigenvector corresponding to λ_1 were recovered from the circuit at the end of the optimization. Our numerical simulations showed an overall improvement in both the accuracy and convergence with VQD-exact0 even for the 4-qubit operator with the same ansätzë. Our findings highlight the importance of constructing an informed initial guess for the state vector to run and extract accurate results from variational quantum algorithms efficiently.

C. Non-Equilibrium Steady State

Here, we report numerical results for the zeromode (i.e., the non-equilibrium steady state) of the stochastic (bistable) Schlögl matrix obtained on `ibm_brisbane`, a 127-qubit QPU. We use QPE to verify if the non-equilibrium steady-state of the stochastic Schlögl model can be recovered on quantum hardware. It is possible to numerically estimate the zeromode (non-equilibrium steady-state) using QPE directly, although we realized that we could not do so accurately due to a failure of QPE to resolve small amplitudes and correctly recover the

(a) 2-qubit monostable operator.

(b) 2-qubit bistable operator.

(c) 3-qubit monostable operator.

(d) 3-qubit bistable operator.

(e) 4-qubit monostable operator using ansätz A.

(f) 4-qubit bistable operator using ansätz A.

(g) 4-qubit monostable operator using ansätz B.
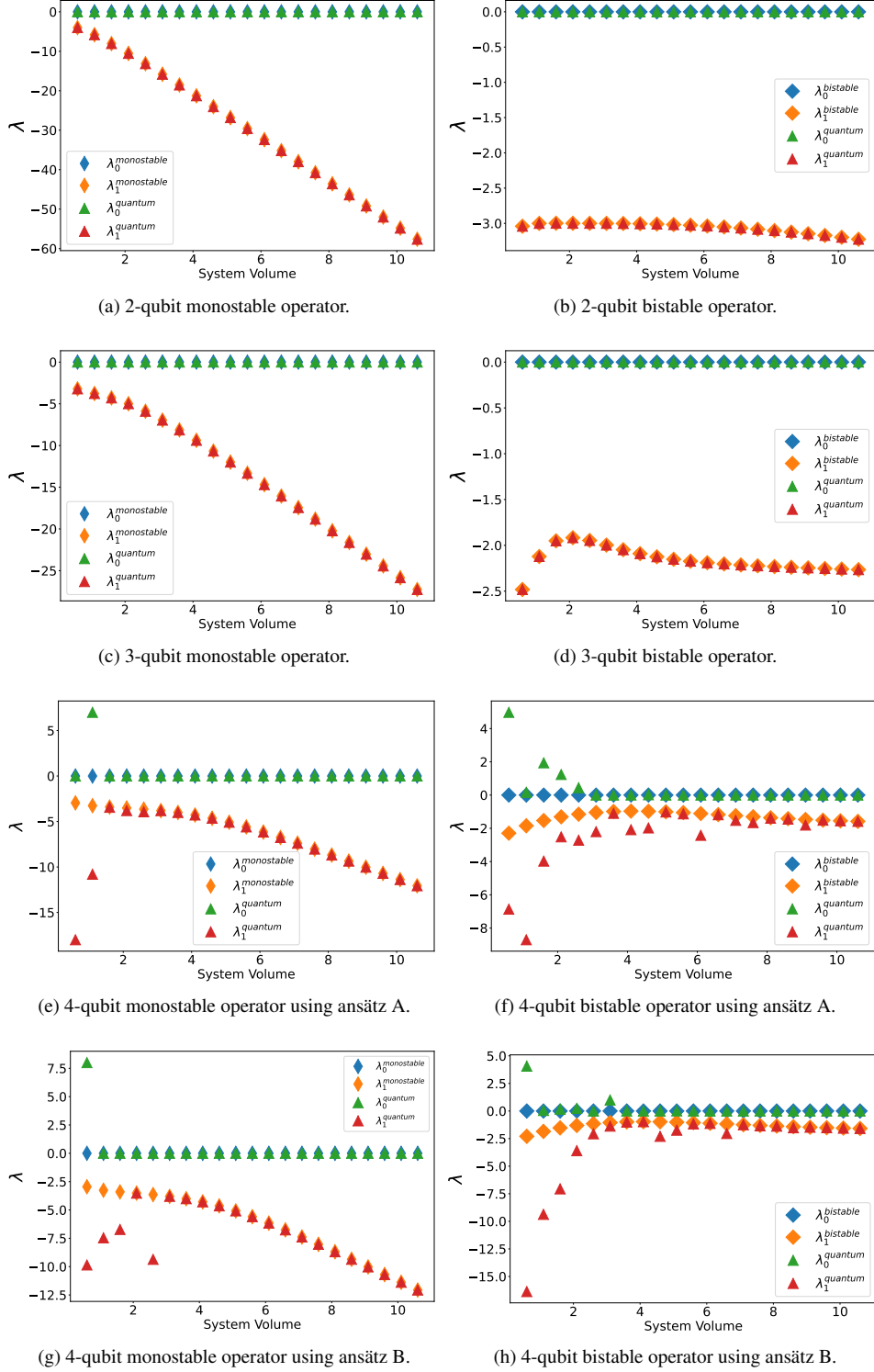
(h) 4-qubit bistable operator using ansätz B.

Figure 5: Quantum versus classical eigenvalues for the monostable and bistable Schlögl operators using 2- ((a) and (b)), 3- ((c) and (d)), and 4- ((e)-(h)) qubit basis sets. The eigenvalues computed using VQD are in excellent agreement with the classically-computed eigenvalues for the 2- and 3-qubit cases. Numerically exact results are obtained for these operators for all system volumes considered. For the 4-qubit operators, two different ansätze sizes, A and B, were used corresponding to the `TwoLocal` ansätz types with 4 and 5 circuit repetitions, respectively. The low accuracy observed for small volumes is likely due to the limited expressivity of the ansätz. Ansätz A performed slightly better than B for these volumes but ansätz B was more stable when the system volume was moderately larger. Details about our ansätz analysis for different operators can be found in the Supplementary Materials.
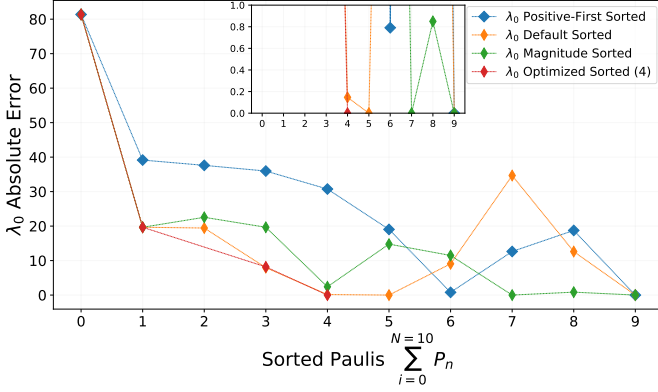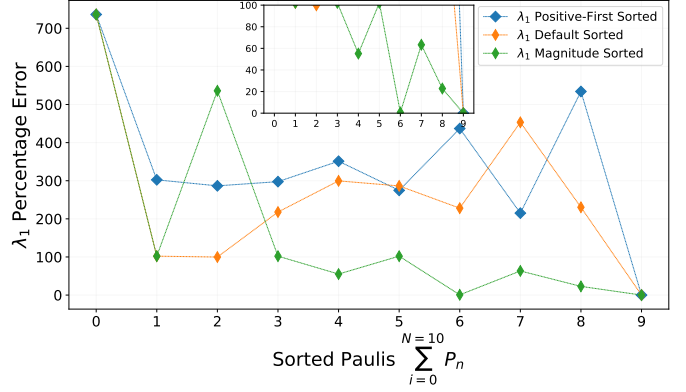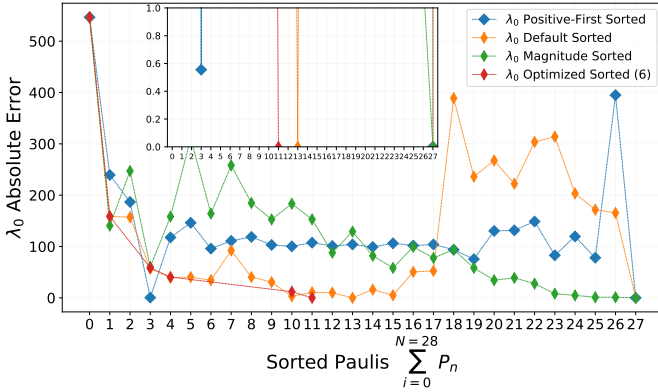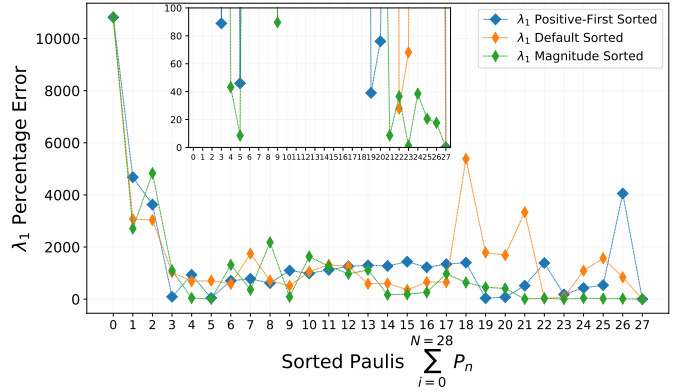
(a) λ_0 from 2-qubit bistable operator.

(b) λ_1 from 2-qubit bistable operator.

(c) λ_0 from 3-qubit bistable operator.

(d) λ_1 from 3-qubit bistable operator.

Figure 6: Error plots for 2- and 3-qubit operators in λ_0 and λ_1 from different Pauli term sorting methods. (a) and (b) show the absolute errors in the estimation of λ_0 while (c) and (d) depict the percentage errors in the estimation of λ_1. The insets have the same units as the main plots. For λ_0, the default sort and optimized sort yield the most accurate results. In the default sort, only half of the terms are required for an exact solution. This is consistent for operators much larger than 3 qubits, and also holds true for the monostable operator. For λ_1, the magnitude sort provided the most reasonable trade-off between accuracy and number of terms used. See Table S4 in the Supplementary Materials.

components of the desired eigenvector, especially in the presence of noise. This is somewhat anticipated given that QPE is expected to become advantageous on future, fault-tolerant hardware, not the near-term hardware used in this work. This prompted us to switch to VQSVD to extract the zeromode of the Schlögl operator instead. We set the number of precision qubits used to construct the QPE circuit equal to seven. In what follows, we present zeromode results for three different system volumes, i.e., $V = 1.1$, $V = 5.5$, and $V = 10.5$, respectively.

In each case, we computed the zeromode using a two-qubit operator, which resulted in a 4×4 stochastic Schlögl matrix. Employing the transformation in Eq. 14 yields an 8×8 matrix, resulting in a basis size of eight. This gave us a query qubit register size of three for the QPE circuit. We compared the zeromodes obtained via exact diagonalization to the ones obtained via the implementation of QPE + VQSVD (details regarding the hyperparameters chosen to run VQSVD may be found in the Supplementary Materials). We construct the

stochastic Schlögl matrix from the CME using the procedure outlined in Sec. II C.

We would like to remark here that a basis size of eight is by no means sufficient to reproduce the full bistable dynamics of the Schlögl model (i.e., the presence of two bistable states in the reaction network). A much larger basis size is needed to achieve this on both classical and quantum computers. To reproduce bistability, at least a 5-qubit representation of the original Schlögl operator (i.e., Equation 10) is needed. This results in a basis vector with at least 32 components. However, since Equation 10 must be brought to its Hermitian form as per Equation 14, an extra qubit is necessary to accommodate a matrix twice as large. Consequently, a basis size of at least 64 (which can be encoded using 6 qubits) would be required to demonstrate bistability. Our goal here is to present results that follow as a proof-of-concept, illustrating the recovery of the non-equilibrium steady state of the Schlögl model on current NISQ hardware, albeit with potentially added overheads
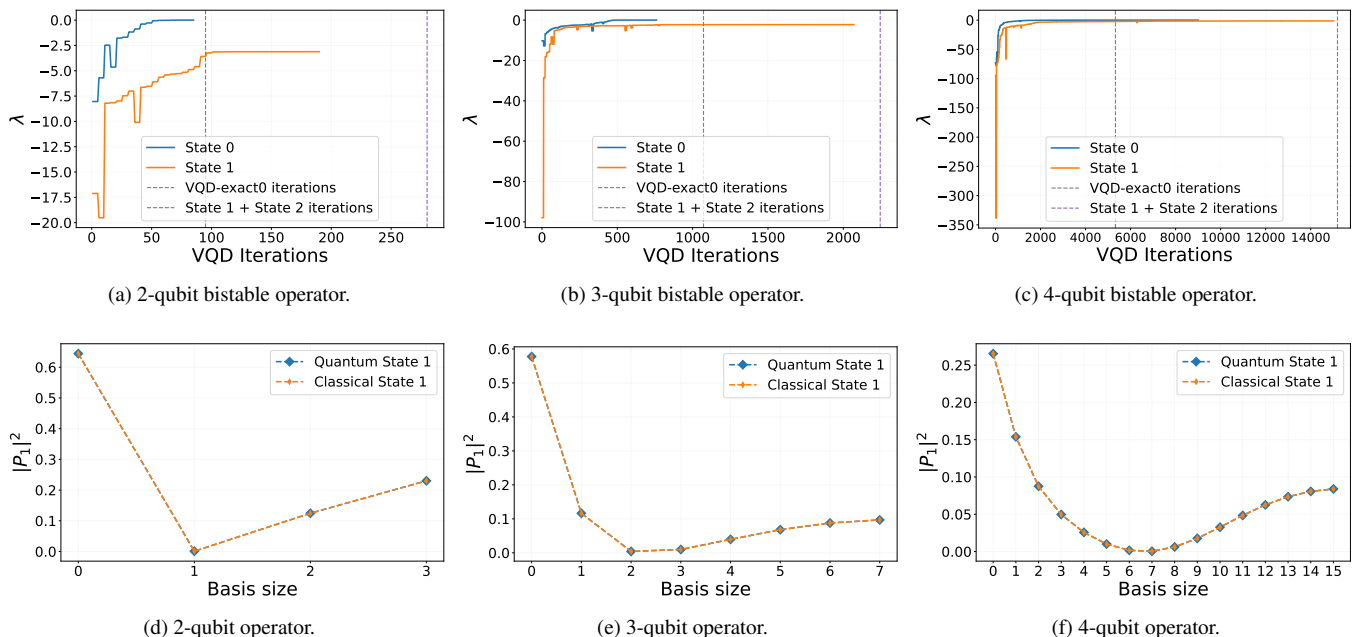
(a) 2-qubit bistable operator.

(b) 3-qubit bistable operator.

(c) 4-qubit bistable operator.

(d) 2-qubit operator.

(e) 3-qubit operator.

(f) 4-qubit operator.

Figure 7: Noiseless simulations with the VQD-`exact0` algorithm. (a)-(c) show VQD iterations and (d)-(f) depict the eigenvectors corresponding to λ_1 for different basis sizes. The purple and black vertical lines represent the total number of iterations for the VQD and VQD-`exact0` algorithms, respectively. Simulations for the 2-, 3-, and for 4-qubit operators with $V = 8.5$ are shown. The number of VQD iterations increases rapidly with the basis size due to the increase in the number of variational parameters to be optimized. For VQD-`exact0`, the iterations can be reduced significantly (by at least half) due to the exact initialization of the first excited state.

and/or resource requirements.

We observe a reasonably good quantitative agreement between the classical and quantum results for each system volume considered [we obtain root-mean-square (RMS) deviation errors between the exact (classical diagonalization) and quantum zeromodes on the order of $3-5\%$ (see the Supplementary Materials for more details)]. As mentioned previously, we employed only half of the basis set to compute the lowest eigenvalue of the stochastic Schlögl matrix and its corresponding zeromode. Therefore, the first four data points in Fig. 8 are irrelevant for our analysis.

To compute the RMS deviation, we use

$$\text{RMSD} = \sqrt{\frac{\sum_{i=1}^{m}\left(y_i^{\text{exact}} - y_i^{\text{quantum}}\right)^2}{m}}, \qquad (21)$$

where y^{exact} (y^{quantum}) denotes the zeromode obtained via exact classical diagonalization (QPE + VQSVD) and m denotes the number of data points over which we sample the distribution (four, in our case).

As a further check, we report results for the steady-state expectation value of the bistable Schlögl operator $\hat{Q}_H$ [i.e., $\langle \hat{Q}_H \rangle = \langle u_0 | \hat{Q}_H | u_0 \rangle$, where $|u_0\rangle$ denotes the non-equilibrium steady-state (zeromode)] for different system volumes in the Supplementary Materials. We expect $\langle \hat{Q}_H \rangle$ to identically vanish with respect to the non-equilibrium steady-state. Barring numerical floating point errors, we obtain values for $\langle \hat{Q}_H \rangle$

very close to zero (i.e., $\sim \mathcal{O}(10^{-4})$). This indicates that the results for the non-equilibrium steady-state we obtain via the implementation of QPE + VQSVD are consistent with the results we obtain via exact diagonalization for different system volumes.

VI. DISCUSSION

In this work, we applied different strategies to analyze the contributions of each term to the full Schlögl operator with the goal of eliminating some of the less important terms. The errors encountered in implementing variational quantum algorithms such as VQD can be mitigated by considering operators with fewer Pauli terms that require fewer measurements. To understand the relevance of each term, we applied different sorting techniques and computed the expectation values of the resulting truncated operators. By employing different sorting techniques, we found that about half of the terms were not required to estimate an exact value of λ_0 for any Schlögl operator constructed by Pauli decomposing Equation 16. Although we only present results for the bistable case in the main text, this was found to be surprisingly true for the monostable operator as well. No symmetry was used to directly reduce the number of gates in the circuit. Instead, the truncation of terms in an operator heavily depended on how the original operator was mapped to qubits. Additionally, no symmetries were

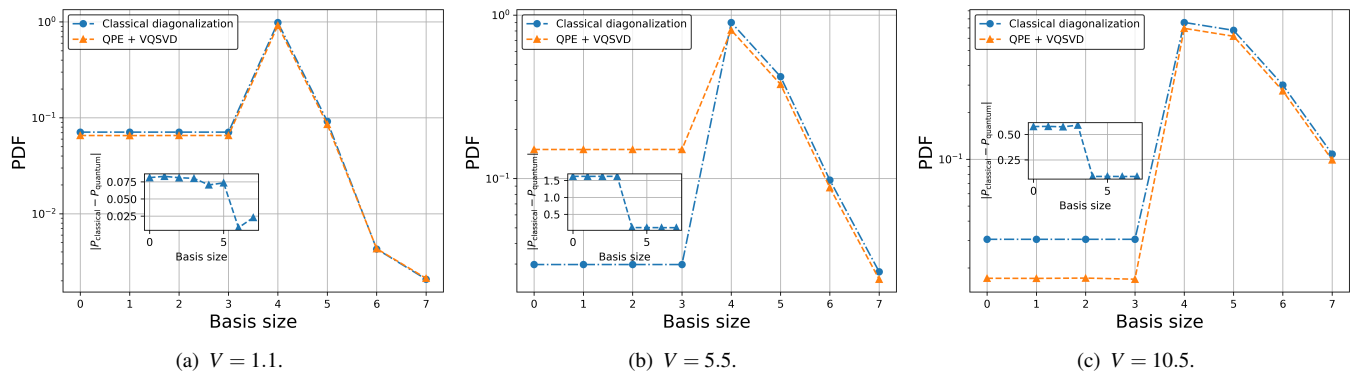(a) $V = 1.1$.　　(b) $V = 5.5$.　　(c) $V = 10.5$.

Figure 8: Plots for the zeromode obtained via exact classical diagonalization and QPE + VQSVD on `ibm_brisbane` for different system volumes. We use three query qubits and seven precision qubits to construct the QPE circuit, respectively. The insets show the absolute error between the classical and quantum zeromodes for each basis size. Note that we plot both zeromodes on a log scale. Only the last four data points are relevant for our quantitative analysis.

identified in the operator for λ_1 that could reliably facilitate a cancellation or omission of terms. However, the magnitude sort yielded a reasonably good trade-off between the error and the number of terms to be dropped from the full operator.

It is worth noting that the symmetries identified in the classical (Hermitian) operator also depend on the transformations used to construct a sparse representation of the operator and on the decomposition employed to express the classical operator as a linear combination of Pauli strings. For example, different sets of Pauli strings may arise with different symmetries, if any, when computing the eigenvalues of Equation 14 versus those of Equation 16. Therefore, investigating how a given operator is mapped to qubits is a crucial step that warrants further exploration for applications pertaining to the simulation of classical systems on near-term quantum hardware.

The greatest computational gains in our simulations were seen using VQD with exact initial conditions, which converged in at least half the number of steps required to converge standard VQD with a naive initial state. This too is consistent with what is known about variational algorithms (both classical and quantum)—their accuracy and efficiency is highly dependent on the quality of that initial "guess." Our work exemplifies this fact and highlights the need to develop improved initial states for the quantum simulation of classical differential equations. The other requirement for quantum computing the eigenvalues for such a system is the existence of a reasonable Hermitian approximation of the system. The first non-zero eigenvalue is an important observable in a lot of physical applications, including stochastic kinetics. It is also very difficult to compute classically for realistic system sizes.[80,81] Developing variational quantum algorithms capable of extracting the lowest non-zero eigenvalue of a physical system will prove to be a fruitful venture.

We implemented QPE + VQSVD on the `ibm_brisbane` QPU to obtain an estimate for the zeromode of the Schlögl operator for different system volumes and observed RMS deviation errors on the order of $3-5\%$. We note, however, that the basis size we used is insufficient to reproduce the bista-

bility dynamics of the Schlögl model. To approach the region of bistability for any given system volume, the use of a much larger basis size is warranted on both classical and quantum computers. Owing to resource constraints on current-NISQ hardware, we argue that the use of large basis sizes (i.e., the simulation of higher-dimensional stochastic Schlögl matrices) on presently available quantum machines remains practically infeasible. It also remains unclear if the variational quantum algorithms employed in this paper (i.e., VQD and VQSVD) promise a quantum advantage. We hope to address this question via a detailed analysis of the scaling of classical versus quantum implementations in a future work.

For the efficient simulation of higher-dimensional stochastic Schlögl matrices on near-term quantum hardware, dimensionality reduction techniques may prove to be useful. We note that a systematic analysis of the number of independent degrees of freedom that VQSVD can efficiently handle (and by extension, the dimension of matrices that it can find the SVD of) is warranted. We suspect that an additional optimization of the existing VQSVD algorithm may be required to enable large-scale simulations.

VII. CONCLUSIONS AND OUTLOOK

In this work, we have demonstrated how an important stochastic differential equation, the Chemical Master Equation, can be solved on quantum hardware using a variety of quantum algorithms suitable for both near-term and future fault-tolerant quantum hardware. In particular, we developed and applied quantum algorithms to compute the first two eigenvalues and the non-equilibrium steady state of the Schlögl model, a paradigmatic example of a trimolecular reaction network known to exhibit multiple equilibrium states, using the VQD, QPE, and VQSVD algorithms, respectively. To do so, we demonstrated how the Schlögl model's stochastic Q matrix can be cast into a Hermitian form amenable to variational quantum eigensolvers and then employed classi-

cal modeling to benchmark which portions of the original non-Hermitian probability distributions can be captured in this way. The model's eigenvalues were subsequently calculated via noiseless and noisy quantum simulations for 2-, 3-, and 4-qubit Schlögl operators. The quantum computed non-equilibrium steady-state agrees within a few percent of the non-equilibrium steady-state obtained via exact diagonalization for all system volumes considered.

In our eigenvalue simulations, various sorting procedures were employed to analyze the contribution of each Pauli string to the expectation value of the full Schlögl operator. For λ_0, we find that the operator can be truncated by at least half without sacrificing accuracy. While no such symmetry was identified for λ_1, sorting the Pauli strings by the magnitude of their coefficients yielded the lowest percentage errors: 0% for the 2-qubit case with a 7/10 truncation ratio, and 1.29% for the 3-qubit operator with a 24/28 truncation ratio. Notably, we numerically identify an exact form of the eigenvector corresponding to the lowest non-zero eigenvalue of the Hermitian Schlögl operator. We use this exact eigenstate as the initial state in our implementation of a modified version of the VQD algorithm, VQD-exact0. Using this exact initialization of the lowest state, we observe a significant reduction in the number of VQD iterations. Using 2-, 3-, and 4-qubit Schlögl operators, we consistently observe at least a 50% reduction in the number of classical optimization iterations.

One of the outstanding challenges for variational quantum algorithms is the accumulation of errors due to the multiple measurements that need to be performed as the classical optimization loop progresses.[10] This means that larger circuits with more parameters will incur more error than smaller circuits. Additionally, larger circuits demand a much more expressive ansätz with more parameters and more qubits. These facts are consistent with our results, as we observed the largest errors in the 4-qubit case.

Reducing the number of measurements, the depth of the quantum circuit, and number of optimization parameters while maintaining accuracy are crucial for scaling variational quantum algorithms to realistic system sizes beyond simplistic toy models. Some classical systems possess operators with symmetries that can be exploited by quantum algorithms, as demonstrated in this paper for the Schlögl model. In our work, we furthermore illustrate the importance of utilizing larger basis set sizes (i.e., higher-dimensional stochastic Schlögl matrices) to reproduce the bistable dynamics of the (bistable) Schlögl model. A smaller basis set is by no means sufficient to reproduce the bistable nature of the non-equilibrium steady-state, as we note in Secs. V C and VI. To achieve this on both classical and quantum hardware, the use of a much larger basis set is warranted (see Sec. VI). Thus, the development of variational quantum algorithms that can efficiently enable the simulation of such higher-dimensional matrices (and related system representations) is in order. We hope that our work spearheads further research in this direction.

There is significant promise in advancing the application of quantum algorithms to classical problems, although this avenue remains underexplored. The zeromode approach allows one to directly target the non-equilibrium steady-state of a classical dynamical system (both deterministic and stochastic in nature). This enables the efficient estimation of relevant observables of interest in the non-equilibrium steady-state. In the context of this approach, we envision a scenario in which a smaller basis version of a classical problem may be analyzed using conventional classical algorithms to understand the form of the Hermitian zeromode of the classical dynamical system in question and the symmetries present therein. This information can subsequently be used to inform the initialization of the initial "guess" (i.e., the initial quantum state) to be fed to a variational quantum algorithm to simulate the classical dynamical system on near-term quantum hardware using a larger basis set.

We emphasize that developing better workflows (and refining existing ones) for solving non-Schrödinger type PDEs such as the CME is in great need. Enhanced initialization schemes are crucial to ensure the convergence and numerical stability of large-scale simulations of non-Schrödinger-type PDEs. Moreover, the development of improved variational quantum algorithms is essential for leveraging quantum computing capabilities to tackle non-Schrödinger-type PDEs efficiently. The pursuit of more exact theoretical and numerical approaches is also essential for achieving higher precision in modeling physical phenomena on near-term quantum hardware accurately.

Our work opens new avenues for using current-NISQ devices as an alternative to classical computation to solve exponentially challenging stochastic chemical kinetics problems. We demonstrate how quantum algorithms can be extended to the simulation of stochastic chemical kinetics, thereby paving the way for new research directions and methodologies in both quantum computing and computational chemistry. It remains to be seen if a quantum advantage can be achieved in modeling stochastic chemical reactions and/or networks on near-term quantum hardware, and we hope that our work inspires further research in this direction.

DATA AND CODE AVAILABILITY

Our Schlögl model GitHub repository contains code to implement the classical and quantum subroutines. Additional

data pertaining to the VQD ansätz and classical optimizer analysis (for VQD) can also be found in the aforementioned repository.

SUPPLEMENTARY MATERIALS

We tabulate all of the data plotted and provide more detailed explanations of our parameter choices in our Supplementary Materials.

REFERENCES

REFERENCES

[1] Zidu Liu, L.-M. Duan, and Dong-Ling Deng. Solving quantum master equations with deep quantum neural networks. *Physical Review Research*, 4(1):013097, February 2022. ISSN 2643-1564. doi:10.1103/PhysRevResearch.4.013097. URL https://link.aps.org/doi/10.1103/PhysRevResearch.4.013097.

[2] Alberto Baiardi, Matthias Christandl, and Markus Reiher. Quantum Computing for Molecular Biology**. *ChemBioChem*, 24(13):e202300120, July 2023. ISSN 1439-4227, 1439-7633. doi:10.1002/cbic.202300120. URL https://chemistry-europe.onlinelibrary.wiley.com/doi/10.1002/cbic.202300120.

[3] Mukhtar Ullah and Olaf Wolkenhauer. Stochastic approaches in systems biology. *WIREs Systems Biology and Medicine*, 2(4):385–397, 2010. ISSN 1939-005X. doi:10.1002/wsbm.78. URL https://onlinelibrary.wiley.com/doi/abs/10.1002/wsbm.78. _eprint: https://onlinelibrary.wiley.com/doi/pdf/10.1002/wsbm.78.

[4] Hao Ge, Min Qian, and Hong Qian. Stochastic theory of nonequilibrium steady states. Part II: Applications in chemical biophysics. *Physics Reports*, 510(3):87–118, January 2012. ISSN 0370-1573. doi:10.1016/j.physrep.2011.09.001. URL https://www.sciencedirect.com/science/article/pii/S0370157311002419.

[5] F. Tennie and T. N. Palmer. Quantum Computers for Weather and Climate Prediction: The Good, the Bad, and the Noisy. *Bulletin of the American Meteorological Society*, 104(2):E488–E500, February 2023. ISSN 0003-0007, 1520-0477. doi:10.1175/BAMS-D-22-0031.1. URL https://journals.ametsoc.org/view/journals/bams/104/2/BAMS-D-22-0031.1.xml.

[6] Miroslav Dobšíček, Göran Johansson, Vitaly Shumeiko, and Göran Wendin. Arbitrary accuracy iterative quantum phase estimation algorithm using a single ancillary qubit: A two-qubit benchmark. *Physical Review A*, 76(3):030306, 2007. Publisher: APS.

[7] Aram W. Harrow, Avinatan Hassidim, and Seth Lloyd. Quantum Algorithm for Linear Systems of Equations. *Physical Review Letters*, 103(15):150502, October 2009. doi:10.1103/PhysRevLett.103.150502. URL https://link.aps.org/doi/10.1103/PhysRevLett.103.150502. Publisher: American Physical Society.

[8] Yudong Cao, Jonathan Romero, Jonathan P. Olson, Matthias Degroote, Peter D. Johnson, Mária Kieferová, Ian D. Kivlichan, Tim Menke, Borja Peropadre, and Nicolas PD Sawaya. Quantum chemistry in the age of quantum computing. *Chemical reviews*, 119(19):10856–10915, 2019. Publisher: ACS Publications.

[9] M. Cerezo, Andrew Arrasmith, Ryan Babbush, Simon C. Benjamin, Suguru Endo, Keisuke Fujii, Jarrod R. McClean, Kosuke Mitarai, Xiao Yuan, Lukasz Cincio, and Patrick J. Coles. Variational quantum algorithms. *Nature Reviews Physics*, 3(9):625–644, September 2021. ISSN 2522-5820. doi:10.1038/s42254-021-00348-9. URL https://www.nature.com/articles/s42254-021-00348-9. Number: 9 Publisher: Nature Publishing Group.

[10] Dmitry A. Fedorov, Bo Peng, Niranjan Govind, and Yuri Alexeev. VQE method: a short survey and recent developments. *Materials Theory*, 6(1):2, January 2022. ISSN 2509-8012. doi:10.1186/s41313-021-00032-6. URL https://doi.org/10.1186/s41313-021-00032-6.

[11] Alberto Peruzzo, Jarrod McClean, Peter Shadbolt, Man-Hong Yung, Xiao-Qi Zhou, Peter J. Love, Alán Aspuru-Guzik, and Jeremy L. O'Brien. A variational eigenvalue solver on a photonic quantum processor. *Nature Communications*, 5(1):4213, July 2014. ISSN 2041-1723. doi:10.1038/ncomms5213. URL https://www.nature.com/articles/ncomms5213. Number: 1 Publisher: Nature Publishing Group.

[12] Jarrod R. McClean, Jonathan Romero, Ryan Babbush, and Alán Aspuru-Guzik. The theory of variational hybrid quantum-classical algorithms. *New Journal of Physics*, 18(2):023023, February 2016. ISSN 1367-2630. doi:10.1088/1367-2630/18/2/023023. URL https://dx.doi.org/10.1088/1367-2630/18/2/023023. Publisher: IOP Publishing.

[13] Jonathan Romero, Ryan Babbush, Jarrod R McClean, Cornelius Hempel, Peter J Love, and Alán Aspuru-Guzik. Strategies for quantum computing molecular energies using the unitary coupled cluster ansatz. *Quantum Science and Technology*, 4(1):014008, 2018. Publisher: IOP Publishing.

[14] Oscar Higgott, Daochen Wang, and Stephen Brierley. Variational Quantum Computation of Excited States. *Quantum*, 3:156, July 2019. ISSN 2521-327X. doi:10.22331/q-2019-07-01-156. URL http://arxiv.org/abs/1805.08138. arXiv:1805.08138 [quant-ph].

[15] Xin Wang, Zhixin Song, and Youle Wang. Variational Quantum Singular Value Decomposition. *Quantum*, 5:483, June 2021. doi:10.22331/q-2021-06-29-483. URL https://quantum-journal.org/papers/q-2021-06-29-483/. Publisher: Verein zur Förderung des Open Access Publizierens in den Quantenwissenschaften.

[16] Abhinav Kandala, Antonio Mezzacapo, Kristan Temme, Maika Takita, Markus Brink, Jerry M Chow, and Jay M Gambetta. Hardware-efficient variational quantum eigensolver for small molecules and quantum magnets. *Nature*, 549(7671):242–246, 2017. Publisher: Nature Publishing Group.

[17] Jules Tilly, Glenn Jones, Hongxiang Chen, Leonard Wossnig, and Edward Grant. Computation of molecular excited states on IBM quantum computers using a discriminative variational quantum eigensolver. *Physical Review A*, 102(6):062425, December 2020. doi:10.1103/PhysRevA.102.062425. URL https://link.aps.org/doi/10.1103/PhysRevA.102.062425. Publisher: American Physical Society.

[18] Jingwei Wen, Zhengan Wang, Chitong Chen, Junxiang Xiao, Hang Li, Ling Qian, Zhiguo Huang, Heng Fan, Shijie Wei, and Guilu Long. A full circuit-based quantum algorithm for excited-states in quantum chemistry. *Quantum*, 8:1219, January 2024. doi:10.22331/q-2024-01-04-1219. URL https://quantum-journal.org/papers/q-2024-01-04-1219/. Publisher: Verein zur Förderung des Open Access Publizierens in den Quantenwissenschaften.

[19] T. Powers and R. M. Rajapakse. Using Variational Eigensolvers on Low-End Hardware to Find the Ground State Energy of Simple Molecules, October 2023. URL http://arxiv.org/abs/2310.19104. arXiv:2310.19104 [quant-ph] version: 1.

[20] Changsu Cao, Jinzhao Sun, Xiao Yuan, Han-Shi Hu, Hung Q. Pham, and Dingshun Lv. Ab initio quantum simulation of strongly correlated materials with quantum embedding. *npj Computational Materials*, 9(1):1–11, May 2023. ISSN 2057-3960. doi:10.1038/s41524-023-01045-0. URL https://www.nature.com/articles/s41524-023-01045-0. Number: 1 Publisher: Nature Publishing Group.

[21] Laura Clinton, Johannes Bausch, and Toby Cubitt. Hamiltonian simulation algorithms for near-term quantum hardware. *Nature Communications*, 12(1):4989, August 2021. ISSN 2041-1723. doi:10.1038/s41467-021-25196-0. URL https://www.nature.com/articles/s41467-021-25196-0.

[22] Giuliano Benenti and Giuliano Strini. Quantum simulation of the single-particle Schrödinger equation. *American Journal of Physics*, 76(7):657–662, July 2008. ISSN 0002-9505. doi:10.1119/1.2894532. URL https://doi.org/10.1119/1.2894532.

[23] William J. Huggins, Bryan A. O'Gorman, Nicholas C. Rubin, David R. Reichman, Ryan Babbush, and Joonho Lee. Unbiasing fermionic quantum Monte Carlo with a quantum computer. *Nature*, 603(7901):416–420, March 2022. ISSN 1476-4687. doi:10.1038/s41586-021-04351-z. URL https://www.nature.com/articles/s41586-021-04351-z. Publisher: Nature Publishing Group.

[24] Scott E. Smart and David A. Mazziotti. Verifiably exact solution of the electronic Schr\"odinger equation on quantum devices. *Physical Review A*, 109(2):022802, February 2024. doi:

10.1103/PhysRevA.109.022802. URL https://link.aps.org/doi/10.1103/PhysRevA.109.022802. Publisher: American Physical Society.

[25] Felix Tennie and Luca Magri. Solving nonlinear differential equations on Quantum Computers: A Fokker-Planck approach, January 2024. URL http://arxiv.org/abs/2401.13500. arXiv:2401.13500 [nlin, physics:physics, physics:quant-ph].

[26] Abeynaya Gnanasekaran, Amit Surana, and Tuhin Sahai. Efficient Quantum Algorithms for Nonlinear Stochastic Dynamical Systems. pages 66–75. IEEE Computer Society, September 2023. ISBN 9798350343236. doi:10.1109/QCE57702.2023.10186. URL https://www.computer.org/csdl/proceedings-article/qce/2023/432302a066/1SuQVi76r1m.

[27] Ryan Babbush, Dominic W. Berry, Robin Kothari, Rolando D. Somma, and Nathan Wiebe. Exponential Quantum Speedup in Simulating Coupled Classical Oscillators. Physical Review X, 13(4):041041, December 2023. doi:10.1103/PhysRevX.13.041041. URL https://link.aps.org/doi/10.1103/PhysRevX.13.041041. Publisher: American Physical Society.

[28] Kenji Kubo, Yuya O. Nakagawa, Suguru Endo, and Shota Nagayama. Variational quantum simulations of stochastic differential equations. Physical Review A, 103(5):052425, May 2021. doi:10.1103/PhysRevA.103.052425. URL https://link.aps.org/doi/10.1103/PhysRevA.103.052425. Publisher: American Physical Society.

[29] Carson C. Chow and Michael A. Buice. Path Integral Methods for Stochastic Differential Equations. The Journal of Mathematical Neuroscience, 5(1):8, December 2015. ISSN 2190-8567. doi:10.1186/s13408-015-0018-5. URL http://www.mathematical-neuroscience.com/content/5/1/8.

[30] Crispin W Gardiner. Handbook of Stochastic Methods: For the Natural and Social Sciences. springer, 2009.

[31] Hannes Risken. Fokker-planck equation. In The Fokker-Planck Equation, pages 63–95. Springer, 1996.

[32] Melissa Vellela and Hong Qian. Stochastic dynamics and non-equilibrium thermodynamics of a bistable chemical system: the Schlögl model revisited. Journal of The Royal Society Interface, 6(39):925–940, October 2009. doi:10.1098/rsif.2008.0476. URL https://royalsocietypublishing.org/doi/10.1098/rsif.2008.0476. Publisher: Royal Society.

[33] Shev Macnamara, Alberto M. Bersani, Kevin Burrage, and Roger B. Sidje. Stochastic chemical kinetics and the total quasi-steady-state assumption: application to the stochastic simulation algorithm and chemical master equation. The Journal of Chemical Physics, 129(9):095105, September 2008. ISSN 1089-7690. doi:10.1063/1.2971036.

[34] Paul Sjöberg, Per Lötstedt, and Johan Elf. Fokker–Planck approximation of the master equation in molecular biology. Computing and Visualization in Science, 12(1):37–50, 2009. Publisher: Springer.

[35] Daniel T. Gillespie. The chemical Langevin equation. The Journal of Chemical Physics, 113(1):297–306, July 2000. ISSN 0021-9606. doi:10.1063/1.481811. URL https://doi.org/10.1063/1.481811.

[36] Verena Wolf, Rushil Goel, Maria Mateescu, and Thomas A Henzinger. Solving the chemical master equation using sliding windows. BMC Systems Biology, 4(1):42, December 2010. ISSN 1752-0509. doi:10.1186/1752-0509-4-42. URL https://bmcsystbiol.biomedcentral.com/articles/10.1186/1752-0509-4-42.

[37] Khanh N Dinh and Roger B Sidje. Understanding the finite state projection and related methods for solving the chemical master equation. Physical Biology, 13(3):035003, May 2016. ISSN 1478-3975. doi:10.1088/1478-3975/13/3/035003. URL https://iopscience.iop.org/article/10.1088/1478-3975/13/3/035003.

[38] Kaan Öcal, Guido Sanguinetti, and Ramon Grima. Model reduction for the Chemical Master Equation: An information-theoretic approach. The Journal of Chemical Physics, 158(11):114113, March 2023. ISSN 0021-9606. doi:10.1063/5.0131445. URL https://doi.org/10.1063/5.0131445.

[39] Ankur Gupta and James B. Rawlings. Comparison of parameter estimation methods in stochastic chemical kinetic models: Examples in systems biology. AIChE Journal, 60(4):1253–1268, 2014. ISSN 1547-5905. doi:10.1002/aic.14409. URL https://onlinelibrary.wiley.com/doi/abs/10.1002/aic.14409. _eprint: https://aiche.onlinelibrary.wiley.com/doi/pdf/10.1002/aic.14409.

[40] Augustinas Sukys, Kaan Öcal, and Ramon Grima. Approximating solutions of the Chemical Master equation using neural networks. iScience, 25(9):105010, September 2022. ISSN 25890042. doi:10.1016/j.isci.2022.105010. URL https://linkinghub.elsevier.com/retrieve/pii/S2589004222012822.

[41] Pierpaolo Pravatto, Davide Castaldo, Federico Gallina, Barbara Fresch, Stefano Corni, and Giorgio J. Moro. Quantum computing for classical problems: variational quantum eigensolver for activated processes. New Journal of Physics, 23(12):123045, December 2021. ISSN 1367-2630. doi:10.1088/1367-2630/ac3ff9. URL https://dx.doi.org/10.1088/1367-2630/ac3ff9. Publisher: IOP Publishing.

[42] Marita Oliv, Andrea Matic, Thomas Messerer, and Jeanette Miriam Lorenz. Evaluating the impact of noise on the performance of the Variational Quantum Eigensolver. 2022. doi:10.48550/ARXIV.2209.12803. URL https://arxiv.org/abs/2209.12803.

[43] Waheeda Saib, Petros Wallden, and Ismail Akhalwaya. The Effect of Noise on the Performance of Variational Algorithms for Quantum Chemistry. In 2021 IEEE International Conference on Quantum Computing and Engineering (QCE), pages 42–53, Broomfield, CO, USA, October 2021. IEEE. ISBN 9781665416917. doi:10.1109/QCE52317.2021.00020. URL https://ieeexplore.ieee.org/document/9605335/.

[44] P. Jordan and E. Wigner. Über das Paulische Äquivalenzverbot. Zeitschrift für Physik, 47(9):631–651, September 1928. ISSN 0044-3328. doi:10.1007/BF01331938. URL https://doi.org/10.1007/BF01331938.

[45] E. Ovrum and M. Hjorth-Jensen. Quantum computation algorithm for many-body studies, May 2007. URL http://arxiv.org/abs/0705.1928. arXiv:0705.1928 [quant-ph].

[46] Andrew Tranter, Peter J. Love, Florian Mintert, and Peter V. Coveney. A Comparison of the Bravyi–Kitaev and Jordan–Wigner Transformations for the Quantum Simulation of Quantum Chemistry. Journal of Chemical Theory and Computation, 14(11):5617–5630, November 2018. ISSN 1549-9618. doi:10.1021/acs.jctc.8b00450. URL https://doi.org/10.1021/acs.jctc.8b00450. Publisher: American Chemical Society.

[47] Sergey B. Bravyi and Alexei Yu. Kitaev. Fermionic Quantum Computation. Annals of Physics, 298(1):210–226, May 2002. ISSN 0003-4916. doi:10.1006/aphy.2002.6254. URL https://www.sciencedirect.com/science/article/pii/S0003491602962548.

[48] Jacob T. Seeley, Martin J. Richard, and Peter J. Love. The Bravyi-Kitaev transformation for quantum computation of electronic structure. The Journal of Chemical Physics, 137(22):224109, December 2012. ISSN 0021-9606. doi:10.1063/1.4768229. URL https://doi.org/10.1063/1.4768229.

[49] Hale F. Trotter. On the product of semi-groups of operators. Proceedings of the American Mathematical Society, 10(4):545–551, 1959. URL https://community.ams.org/journals/proc/1959-010-04/S0002-9939-1959-0108732-6/S0002-9939-1959-0108732-6.pdf.

[50] L.-A. Wu, M. S. Byrd, and D. A. Lidar. Polynomial-Time Simulation of Pairing Models on a Quantum Computer. Physical Review Letters, 89(5):057904, July 2002. doi:10.1103/PhysRevLett.89.057904. URL https://link.aps.org/doi/10.1103/PhysRevLett.89.057904. Publisher: American Physical Society.

[51] Vivek V. Shende, Stephen S. Bullock, and Igor L. Markov. Recognizing Small-Circuit Structure in Two-Qubit Operators and Timing Hamiltonians to Compute Controlled-Not Gates. Physical Review A, 70(1):012310, July 2004. ISSN 1050-2947, 1094-1622. doi:10.1103/PhysRevA.70.012310. URL http://arxiv.org/abs/quant-ph/0308045. arXiv:quant-ph/0308045.

[52] Grant Kluber. Trotterization in Quantum Theory, October 2023. URL http://arxiv.org/abs/2310.13296. arXiv:2310.13296 [math-ph, physics:quant-ph].

[53] Yifan Li, Jiaqi Hu, Xiao-Ming Zhang, Zhigang Song, and Man-Hong Yung. Variational Quantum Simulation for Quantum Chemistry. Advanced Theory and Simulations, 2(4):1800182, 2019. ISSN 2513-0390. doi:10.1002/adts.201800182. URL https://onlinelibrary.wiley.com/doi/abs/10.1002/adts.201800182. _eprint: https://onlinelibrary.wiley.com/doi/pdf/10.1002/adts.201800182.

[54] Harper R. Grimsley, Sophia E. Economou, Edwin Barnes, and Nicholas J. Mayhall. An adaptive variational algorithm for exact molecular simulations on a quantum computer. Nature Communications, 10(1):3007, July 2019.

ISSN 2041-1723. doi:10.1038/s41467-019-10988-2. URL https://www.nature.com/articles/s41467-019-10988-2. Number: 1 Publisher: Nature Publishing Group.

[55] F. Schlögl. Chemical reaction models for non-equilibrium phase transitions. *Zeitschrift für Physik*, 253(2):147–161, April 1972. ISSN 0044-3328. doi:10.1007/BF01379769. URL https://doi.org/10.1007/BF01379769.

[56] William J. Blake, Mads KÆrn, Charles R. Cantor, and J. J. Collins. Noise in eukaryotic gene expression. *Nature*, 422(6932):633–637, April 2003. ISSN 1476-4687. doi:10.1038/nature01546. URL https://www.nature.com/articles/nature01546. Number: 6932 Publisher: Nature Publishing Group.

[57] Don Kulasiri and Rahul Kosarwal. *Chemical Master Equation for Large Biological Networks: State-space Expansion Methods Using AI*. Springer, Singapore, 2021. ISBN 9789811653506 9789811653513. doi:10.1007/978-981-16-5351-3. URL https://link.springer.com/10.1007/978-981-16-5351-3.

[58] Nina Fedoroff and Walter Fontana. Small Numbers of Big Molecules. *Science*, 297(5584):1129–1131, August 2002. doi:10.1126/science.1075988. URL https://www.science.org/doi/10.1126/science.1075988. Publisher: American Association for the Advancement of Science.

[59] Thomas Eissing, Holger Conzelmann, Ernst D. Gilles, Frank Allgöwer, Eric Bullinger, and Peter Scheurich. Bistability analyses of a caspase activation model for receptor-induced apoptosis. *The Journal of Biological Chemistry*, 279(35):36892–36897, August 2004. ISSN 0021-9258. doi:10.1074/jbc.M404893200.

[60] Lukas Einkemmer, Julian Mangott, and Martina Prugger. A low-rank complexity reduction algorithm for the high-dimensional kinetic chemical master equation. *Journal of Computational Physics*, 503:112827, April 2024. ISSN 00219991. doi:10.1016/j.jcp.2024.112827. URL https://linkinghub.elsevier.com/retrieve/pii/S0021999124000767.

[61] Daniel T. Gillespie. The Chemical Langevin and Fokker-Planck Equations for the Reversible Isomerization Reaction. *The Journal of Physical Chemistry A*, 106(20):5063–5071, May 2002. ISSN 1089-5639. doi:10.1021/jp0128832. URL https://doi.org/10.1021/jp0128832. Publisher: American Chemical Society.

[62] Daniel T. Gillespie. Exact stochastic simulation of coupled chemical reactions. *The Journal of Physical Chemistry*, 81(25):2340–2361, December 1977. ISSN 0022-3654. doi:10.1021/j100540a008. URL https://doi.org/10.1021/j100540a008. Publisher: American Chemical Society.

[63] Bernard Gaveau, Michael Moreau, and Janos Toth. Master Equation and Fokker–Planck Equation: Comparison of Entropy and of Rate Constants. *Letters in Mathematical Physics*, 40(2):101–115, April 1997. ISSN 1573-0530. doi:10.1023/A:1007362811930. URL https://doi.org/10.1023/A:1007362811930.

[64] Ramon Grima, Philipp Thomas, and Arthur V. Straube. How accurate are the nonlinear chemical Fokker-Planck and chemical Langevin equations? *The Journal of Chemical Physics*, 135(8):084103, August 2011. ISSN 0021-9606. doi:10.1063/1.3625958. URL https://doi.org/10.1063/1.3625958.

[65] N. G. van Kampen. The validity of nonlinear Langevin equations. *Journal of Statistical Physics*, 25(3):431–442, July 1981. ISSN 1572-9613. doi:10.1007/BF01010798. URL https://doi.org/10.1007/BF01010798.

[66] Daniel T. Gillespie. A rigorous derivation of the chemical master equation. *Physica A: Statistical Mechanics and its Applications*, 188(1):404–425, September 1992. ISSN 0378-4371. doi:10.1016/0378-4371(92)90283-V. URL https://www.sciencedirect.com/science/article/pii/037843719290283V.

[67] Silvana Ilie, W.H. Enright, and Kenneth Jackson. Numerical solution of stochastic models of biochemical kinetics. *The Canadian Applied Mathematics Quarterly*, 17, January 2009.

[68] Hong Qian and Hao Ge. Kinetic Rate Equations and the Law of Mass Action. In Hong Qian and Hao Ge, editors, *Stochastic Chemical Reaction Systems in Biology*, Lecture Notes on Mathematical Modelling in the Life Sciences, pages 17–40. Springer International Publishing, Cham, 2021. ISBN 978-3-030-86252-7. doi:10.1007/978-3-030-86252-7_2. URL https://doi.org/10.1007/978-3-030-86252-7_2.

[69] Peter Hanggi, Hermann Grabert, Peter Talkner, and Harry Thomas. Bistable systems: Master equation versus Fokker-Planck modeling. *Physical Review A*, 29(1):371–378, January 1984. doi:10.1103/PhysRevA.29.371. URL https://link.aps.org/doi/10.1103/PhysRevA.29.371. Publisher: American Physical Society.

[70] Richard Bellman and Robert Kalaba. Dynamic programming and statistical communication theory. *Proceedings of the National Academy of Sciences*, 43(8):749–751, August 1957. doi:10.1073/pnas.43.8.749. URL https://www.pnas.org/doi/abs/10.1073/pnas.43.8.749. Publisher: Proceedings of the National Academy of Sciences.

[71] Daochen Wang, Oscar Higgott, and Stephen Brierley. Accelerated Variational Quantum Eigensolver. *Physical Review Letters*, 122(14):140504, April 2019. doi:10.1103/PhysRevLett.122.140504. URL https://link.aps.org/doi/10.1103/PhysRevLett.122.140504. Publisher: American Physical Society.

[72] A. Yu. Kitaev. Quantum measurements and the Abelian Stabilizer Problem. 1995. doi:10.48550/ARXIV.QUANT-PH/9511026. URL https://arxiv.org/abs/quant-ph/9511026.

[73] Matthew Treinish. Qiskit/qiskit-metapackage: Qiskit 0.44.0, July 2023. URL https://zenodo.org/record/2573505.

[74] Ciyou Zhu, Richard H. Byrd, Peihuang Lu, and Jorge Nocedal. Algorithm 778: L-BFGS-B: Fortran Subroutines for Large-Scale Bound-Constrained Optimization. *ACM Transactions on Mathematical Software*, 23(4):550–560, December 1997. ISSN 0098-3500. doi:10.1145/279232.279236. URL http://www.scopus.com/inward/record.url?scp=0031345518&partnerID=8YFLogxK.

[75] Release Paddle Quantum 2.4.0 · PaddlePaddle/Quantum, . URL https://github.com/PaddlePaddle/Quantum/releases/tag/v2.4.0.

[76] PaddlePaddle, . URL https://github.com/PaddlePaddle.

[77] Ran Bi, Tongtong Xu, Mingxue Xu, and Enhong Chen. PaddlePaddle: A Production-Oriented Deep Learning Platform Facilitating the Competency of Enterprises. In *2022 IEEE 24th Int Conf on High Performance Computing & Communications; 8th Int Conf on Data Science & Systems; 20th Int Conf on Smart City; 8th Int Conf on Dependability in Sensor, Cloud & Big Data Systems & Application (HPCC/DSS/SmartCity/DependSys)*, pages 92–99, Hainan, China, December 2022. IEEE. ISBN 9798350319934. doi:10.1109/HPCC-DSS-SmartCity-DependSys57074.2022.00046. URL https://ieeexplore.ieee.org/document/10074745/.

[78] William J. Heuett and Hong Qian. Grand canonical Markov model: A stochastic theory for open nonequilibrium biochemical networks. *The Journal of Chemical Physics*, 124(4):044110, January 2006. ISSN 0021-9606. doi:10.1063/1.2165193. URL https://doi.org/10.1063/1.2165193.

[79] Jules Tilly, Hongxiang Chen, Shuxiang Cao, Dario Picozzi, Kanav Setia, Ying Li, Edward Grant, Leonard Wossnig, Ivan Rungger, George H. Booth, and Jonathan Tennyson. The Variational Quantum Eigensolver: A review of methods and best practices. *Physics Reports*, 986:1–128, November 2022. ISSN 0370-1573. doi:10.1016/j.physrep.2022.08.003. URL https://www.sciencedirect.com/science/article/pii/S0370157322003118.

[80] Marc Bernstein and Lowell S. Brown. Supersymmetry and the Bistable Fokker-Planck Equation. *Physical Review Letters*, 52(22):1933–1935, May 1984. doi:10.1103/PhysRevLett.52.1933. URL https://link.aps.org/doi/10.1103/PhysRevLett.52.1933. Publisher: American Physical Society.

[81] Yu P Kalmykov. Evaluation of the smallest nonvanishing eigenvalue of the Fokker-Planck equation for the Brownian motion in a potential. II. The matrix continued fraction approach. *Physical Review E*, 62(1):227, 2000. Publisher: APS.

Supplementary Materials — Modeling Stochastic Chemical Kinetics on Quantum Computers

Tilas Kabengele[1,2], Yash M. Lokare[3], J. B. Marston[3,4], and Brenda M. Rubenstein[1,3]

[1]*Department of Chemistry, Brown University, Providence, Rhode Island 02912, USA*
[2]*School of Engineering, Brown University, Providence, Rhode Island 02912, USA*
[3]*Department of Physics, Brown University, Providence, Rhode Island 02912, USA*
[4]*Brown Theoretical Physics Center, Brown University, Providence, Rhode Island 02912, USA*

1 Qiskit Software Versions

1.1 VQD Implementation

The Qiskit software versions used to implement VQD on local simulators are as reported below:

Qiskit software	Version
qiskit	0.44.1
qiskit-terra	0.25.1
python	3.10.12
qiskit-algorithms	0.1.0

We used the `poetry Python` version package management system to manage all package dependencies. The `.toml` file can be found on the GitHub repository along with the computer code generated to run numerical simulations and/or experiments.

1.2 QPE + VQSVD Implementation

The Qiskit software versions used to implement the QPE and VQSVD subroutines on `ibm_brisbane` are as reported below:

Qiskit software	Version
`qiskit-terra`	0.24.0
`qiskit-aer`	0.12.0
`qiskit-ibmq-provider`	0.20.2
`qiskit`	0.43.0

2 Non-Equilibrium Steady State (Stochastic Bistable Schlögl Matrix)

2.1 $V = 1.1$

2.1.1 QPE + VQSVD results — `ibm_brisbane`

- Number of experimental shots: 5×10^5; number of precision qubits: 7; number of query qubits: 3.

- **Parameters set for training the quantum neural networks**:

  1. Classical optimizer: Adam optimizer
  2. Number of classical optimization iterations: 200
  3. Learning rate: 0.02
  4. Circuit depth: 55
  5. Weights for VQSVD: [24, 21, 18, 15, 12, 9, 6, 3]

2.1.2 Numerical results

- **RMS deviation (classical and quantum zeromodes)**: 3.375%.

- $\langle \hat{Q}_H \rangle_{|\psi_0\rangle}$: -4.54×10^{-4} (here, $|\psi_0\rangle$ denotes the non-equilibrium steady-state).

2.1.3 Minimum eigenvalue of the Schlögl operator matrix extracted using QPE

$\lambda_{\min}$	
$\lambda_{\text{Schlögl}}$	λ_{unitary}
0.05	0.999 + 0.04j

Table S1: Minimum eigenvalue of the Schlögl operator matrix extracted using QPE.

2.2 $V = 5.5$

2.2.1 QPE + VQSVD results — `ibm_brisbane`

- Number of experimental shots: 5×10^5; number of precision qubits: 7; number of query qubits: 3.

- **Parameters set for training the quantum neural networks**:

  1. Classical optimizer: Adam optimizer
  2. Number of classical optimization iterations: 200

3. Learning rate: 0.02
4. Circuit depth: 55
5. Weights for VQSVD: [24, 21, 18, 15, 12, 9, 6, 3]

2.2.2 Numerical results

- **RMS deviation (classical and quantum zeromodes)**: 5.141%.

- $\langle \hat{Q}_H \rangle_{|\psi_0\rangle}$: 1.47×10^{-4} (here, $|\psi_0\rangle$ denotes the non-equilibrium steady-state).

2.2.3 Minimum eigenvalue of the Schlögl operator matrix extracted using QPE

$\lambda_{\min}$	
$\lambda_{\text{Schlögl}}$	λ_{unitary}
0.04	0.999 + 0.05j

Table S2: Minimum eigenvalue of the Schlögl operator matrix extracted using QPE.

2.3 $V = 10.5$

2.3.1 QPE + VQSVD results — `ibm_brisbane`

- Number of experimental shots: 5×10^5; number of precision qubits: 7; number of query qubits: 3.

- **Parameters set for training the quantum neural networks**:

  1. Classical optimizer: Adam optimizer
  2. Number of classical optimization iterations: 200
  3. Learning rate: 0.02
  4. Circuit depth: 55
  5. Weights for VQSVD: [24, 21, 18, 15, 12, 9, 6, 3]

2.3.2 Numerical results

- **RMS deviation (classical and quantum zeromodes)**: 4.454%.

- $\langle \hat{Q}_H \rangle_{|\psi_0\rangle}$: 3.24×10^{-4} (here, $|\psi_0\rangle$ denotes the non-equilibrium steady-state).

2.3.3 Minimum eigenvalue of the Schlögl operator matrix extracted using QPE

$\lambda_{\min}$	
$\lambda_{\text{Schlögl}}$	λ_{unitary}
0.03	0.999 + 0.03j

Table S3: Minimum eigenvalue of the Schlögl operator matrix extracted using QPE.

2.4   Loss Curves for VQD with Exact Initial State (VQD-exact0)
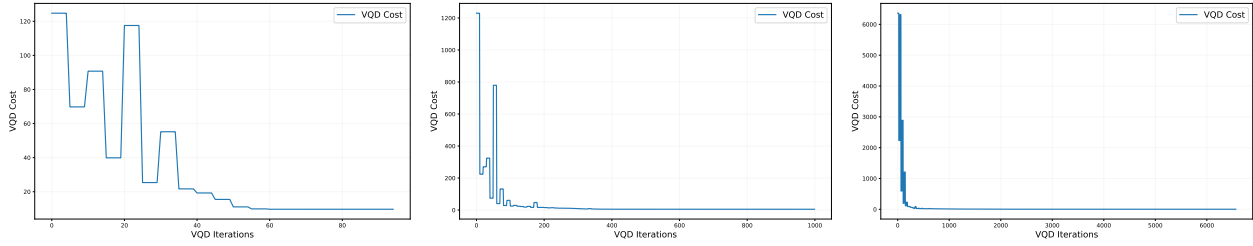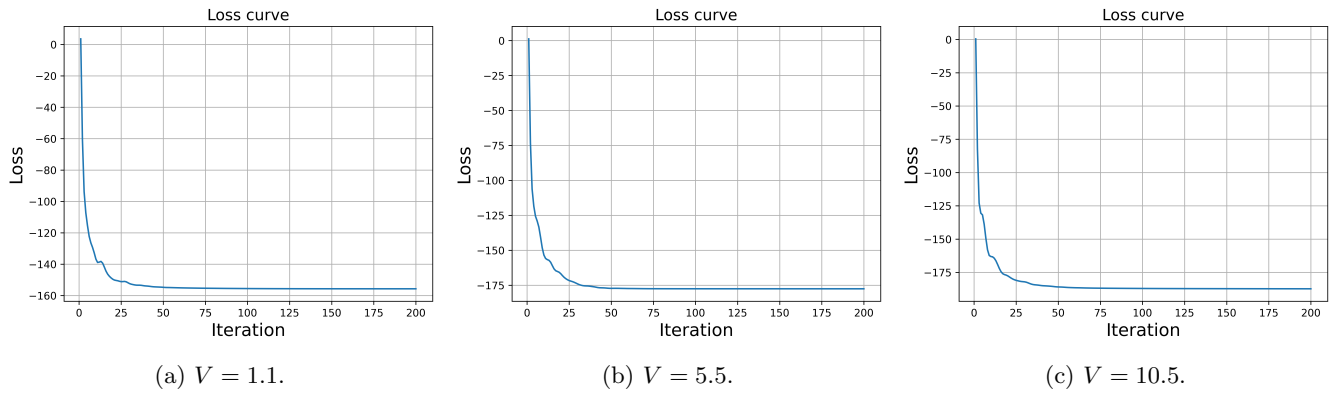

Figure S1: Minimization of the VQD cost function for different qubit bistable operators. (a) VQD-exact0 cost with 2-qubit bistable operator. (b) VQD-exact0 cost with 3-qubit bistable operator. (c) VQD-exact0 with 4-qubit bistable operator.

2.5   Loss Curves (VQSVD)

(a) $V = 1.1$.   (b) $V = 5.5$.   (c) $V = 10.5$.

Figure S2: Minimization of the VQSVD cost function for different system volumes (simulations run on ibm_brisbane).

4

2.6 Percentage Error for Eigenvalues Table

Operator	Positive-First Sort	Default Sort	Magnitude Sort	Optimized Sort
2-qubit λ_0	0.00 (10) 0.79 (7)	0.00 (10) 0.00 (6)	0.00 (10) 0.00 (8)	− 0.00 (4)
2-qubit λ_1	0.00 (10) −	0.00 (10) −	0.00 (10) 0.00 (7)	− −
3-qubit λ_0	0.00 (28) 0.55 (4)	0.00 (14) −	0.00 (28) −	0.00 (6) −
3-qubit λ_1	0.00 (28) 39.06 (20)	0.00 (28) 27.77 (23)	0.00 (28) 1.29 (24)	− −

Table S4: Percentage error in λ_0 and λ_1 for the 2- and 3-qubit operators. For each qubit case, the first row represents results from the full operator while the second row denotes results from the respective truncation method. "−" means that the error in the respective truncation method was significant, i.e., larger than 100%. The digits in parentheses denote the number of Pauli terms used in the operator. The best absolute error and percentage error for λ_0 and λ_1 is given for each truncation method of the full operator. The error plots supporting this table are shown in Figure 5 in the main text.